WPI

Formation of Vesicles in Lipid-Liquid Crystal

Colloidal Mixtures

Submitted to the Faculty of the

WORCESTER POLYTECHNIC INSTITUTE

in partial fulfillment of the requirements for the

Degree of Master of Science

By

Jeffrey D. Peters

Date: April 30, 2014

APPROVED:

Professor Germano S. Iannacchione, Department of Physics, WPI, Advisor

Professor Izabela Stroe, Department of Physics, WPI, Reader

Abstract

The formation, phase ordering, and evolution has been studied in lipid and liquid crystal (LC) colloidal aqueous mixtures as a function of LC concentration and thermal history. The lipid used was 2-oleoyl-1-palmitoyl-sn-glycero-3-phosphocholine (POPC) while the liquid crystal was pentylcyanobiphenyl (5CB). POPC is a naturally occurring lipid in eukaryotic cell membranes and mimics many of the properties of human cell walls. 5CB is a polar liquid crystal that exhibits a thermodynamically stable orientationally ordered (nematic) state at room temperature. Colloidal dispersions were made at various 5CB and POPC concentrations in water and studied via optical microscopy (phase contrast, confocal, florescence, and cross-polarizing) to probe phase order and evolution as well as by calorimetry to study phase transformations. Very large vesicles (>100 μm) were observed to form that appear to use the phase separated 5CB droplets as scaffolds. Also, there appears a unique promotion of dye (used to image the lipid bilayers) crystallization within liquid crystal domains well above room temperature.

Acknowledgements

I would like to thank my advisor, Professor Germano Iannacchione, for his continued support throughout this project. His insight was always welcomed and valuable. I would also like to thank Professor Izabela Stroe for reading my paper and taking part in my defense committee. I would finally like to thank the Worcester Polytechnic Institute Physics Department for the funding necessary to complete this project.

Contents

List of Tables

List of Figures

1   Introduction

1.1   The Role of Lipid Vesicles in Biophysical Research

Living organisms are extremely complex, so to better understand the fundamental mechanisms involved in biological applications, scientists often create less complex models to study. In some cellular research, model cell membranes are created to mimic the basic properties of a cell [1]. Cell walls consist of phospholipids, which when in an aqueous environment, self-assemble in to bilayers which can form spherical vesicles, known as liposomes [2]. Liposomes are divided in to three categories based on size, small (20-50 nm), large (50-100 nm) and giant (10-100 μm) [1]. Small and large vesicles are usually prepared by dissolving lipids in organic solvents, evaporated, buffered, and ultrasonicated. To form giant vesicles, lipid films are dried under an oscillating electric field, a process known as electroformation [3]. Giant vesicles best represent the size of living cells, however, without special equipment it is difficult to create vesicles of this size.

1.2   Liquid Crystal Applications and Research

Phosopholipids are an example of a lyotropic liquid crystal [4]. Liquid crystals exhibit intermediate phase behavior between liquid and crystalline states, as the name would suggest. Another group of liquid crystals are the thermotropic liquid crystals, which change phases according to temperature. In addition to intermediate phases, liquid crystals have unique electro-optic properties. These properties have lead to applications of liquid crystals for temperature sensors, high resolution displays, optical computing, and high strength fibers among others [5].

1.3   Thesis Overview

The goal of this project was to devise a technique to easily produce giant lipid vesicles by utilizing the properties of liquid crystals. POPC lipid membranes were created by using

radially nematic ordered droplets of 5CB liquid crystal as supporting structures. When 5CB is in the isotropic phase (above 35 °C) it has similar physical properties of water. Therefore, a vesicle created with 5CB would behave similarly to a cell containing water. Once the sample preparation procedure was established, experiments were conducted to observe the self-assembly behavior of the lipids and vesicle size distribution. Also, experiments were conducted to compare the behavior of the liquid crystal to its bulk properties. The techniques used for this research included phase contrast, fluorescent, and cross-polarized microscopy as well as modulated differential scanning calorimetry. The thesis resulted in a new procedure for creating giant lipid vesicles and discovery of some unique phenomena arising from the phase ordering of the liquid crystals and lipids.

2 Literature Review

2.1 Liquid Crystals

The term "liquid crystal" describes a state of aggregation that is between a liquid and crystalline solid [4]. A requirement for this mesomorphic behavior is that the molecule must have a highly anisotropic geometry, such as a rod or disk. A typical liquid crystal, such as 5CB, will have an aspect ratio (length to width ratio) of 4, and can be modeled by ellipsoids [6]. Liquid crystals can be divided in two categories: thermotropic liquid crystals, which change phases due to thermal processes, and lyotropic liquid crystals, which change phases by the influences of solvents.

2.1.1 Phases of Liquid Crystals

Thermotropic liquid crystals are classified in three types: nematic, cholesteric and smectic. Nematic liquid crystals have high long-range orientation order, or director, but no translational order, as shown in Figure 2.1
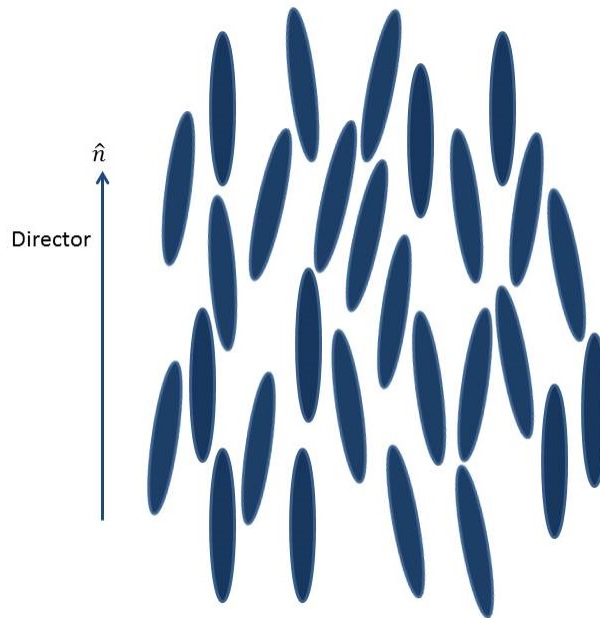
Figure 2.1: A cartoon of the nematic phase of thermotropic liquid crystal.

When the nematic phase has helically oriented directors about an axis, this is what is known as a cholesteric phase. An image of this phase is shown in Figure 2.2.
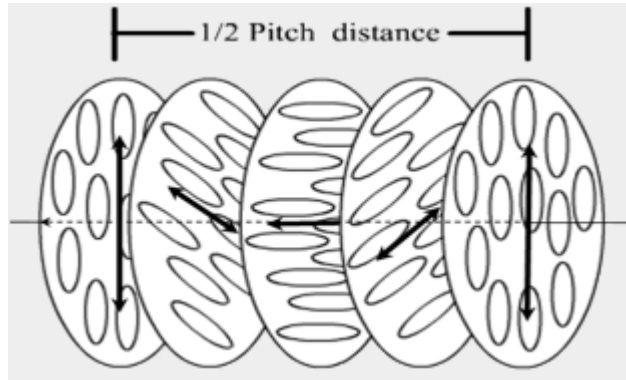
Figure 2.2: A cartoon of the cholesteric liquid crystal phase of thermotropic liquid crystal[7].

Having higher orientational ordering are the smectic phases. The two main phases are known as smectic-A and smectic-C, however, over a dozen of other smectic modifications have be found. Smectic liquid crystals also have translational ordering, allowing the formation of layers which slide over each other fairly easily. In the smectic-A phase, the director is perpendicular to the smectic plane, as can be seen in Figure 2.3.
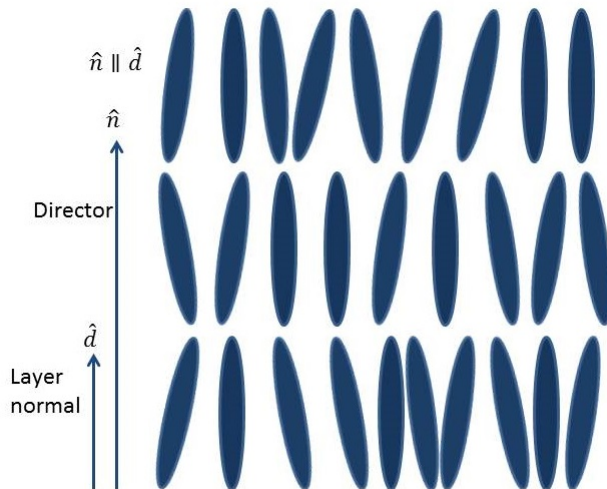
Figure 2.3: A cartoon of the smectic-A phase of thermotropic liquid crystal.

Similarly, the smectic-C phase is a tilted version of the smectic-A phase. A visualization of which can be found in Figure 2.4.
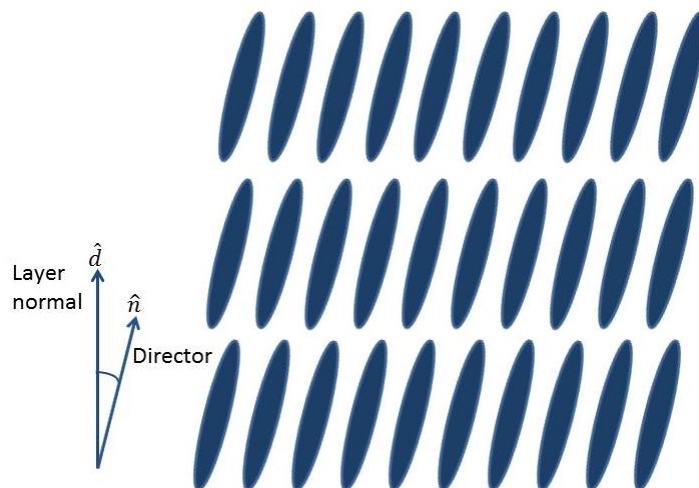
Figure 2.4: A cartoon of the smectic-C phase of thermotropic liquid crystal.

2.1.2 4-Cyano-4'-pentylbiphenyl (5CB)

4-Cyano-4'-pentylbiphenyl (5CB) is one of the most studied liquid crystals [8]. It is in the nematic phase at room temperature and transitions in to the isotropic phase at 35°C. Characteristics of this type of liquid crystal, such as weak absorption in the visible range, chemical stability, dielectric and optical anisotropy, and stable mesophases are due to the physical properties of cyanobiphenyls. 5CB has a rigid cyanobiphenyl head group, and a long, oily tail group. This leads to a dipole moment along a large angle [4]. A model of 5CB can be seen in Figure 2.5.
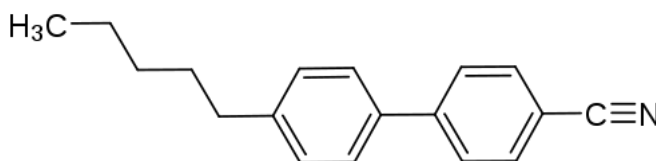
Figure 2.5: A drawing of a 4-Cyano-4'-pentylbiphenyl (5CB) molecule.

2.2 Phospholipids

Phospholipids are the dominant lipids in biomembranes [9]. They are composed of hydrophobic tails and hydrophilic head groups, as shown in Figure 2.6.
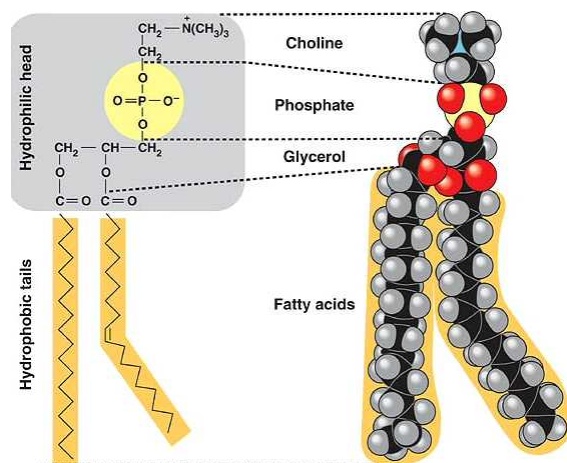
Figure 2.6: Drawing of phospholipid molecule[10].

Phosphatidylcholine is the most common phospholipid, and its inter-lipid interactions are governed by a strong dipole moment. In an aqueous environment, hydrophobic interactions lead to the self-assembly of lipid bilayers. When these bilayers are formed in to a spherical vesicle, they are known as a liposome, as shown in Figure 2.7.
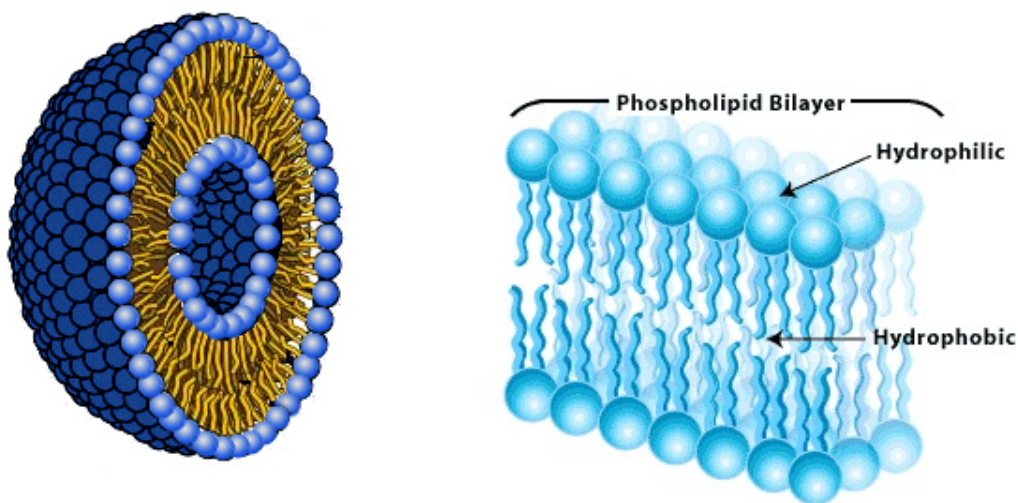
(a) Liposome [11]

(b) Lipid bilayer [12]

Figure 2.7: Cartoon diagram of structure of liposomes and lipid bilayers.

Lipid bilayers show interesting phase behavior, going through liquid, gel, and solid states, making phospholipids a type of lyotropic liquid crystal.

Several techniques for creating lipid vesicles are commonly used, including sonication and extrusion [13]. Extrusion procedures are often implemented using porous polycarbonate membranes, leading to membrane sizes ranging from 100 - 200 nm in size [14]. Similar sizes result from sonication procedures.

2.3 Modulated Differential Scanning Calorimetry

Calorimetry is one of the oldest areas of physical chemistry, dating back to the late 18th century [15]. A calorimeter is an instrument that determines thermal signatures of a sample by directly measuring the temperature. Differential scanning calorimetry (DSC) is a technique in which a sample pan and reference pan are both simultaneously provided the same amount of heat [6]. Therefore any difference in heat flow out of the system is due to the sample and not the pan.Applications of DSC include measuring glass transitions, melting temperatures, heat of fusion, phase transitions, curing kinetics, among many others.

Further improving upon this method is a similar technique, modulated differential scanning calorimetry (MDSC). The first explicit model for MDSC was first introduced by Gobrecht et al. and later improved upon by Reading in 1993 [16] MDSC differs from conventional DSC as a periodic temperature modulation is superimposed on a constant heating scan [17]. This equation governing heat flow in MDSC is given by Equation 2.1.

$$\frac{dH}{dT} = C_p \frac{dT}{dt} + f(T, t) \tag{2.1}$$

Here, dH/DT is the heat flow signal, C_p is the sample heat capacity, dT/dt is the heating rate, and $f(T, t)$ is heat flow as a function of temperature and time. Although the functional dependence allows for the temperature to be modulated by any complex modulating function, sinusoidal oscillations are often chosen, as shown in Figure 2.8.
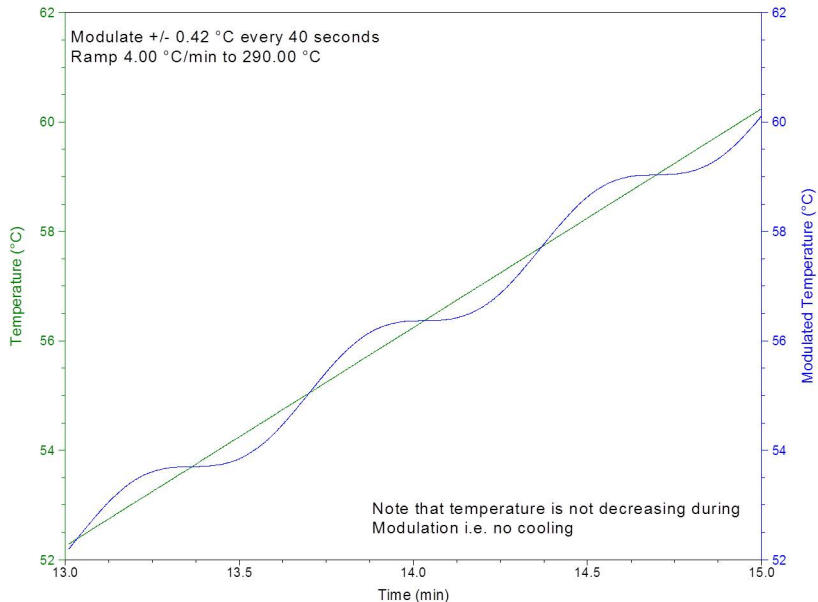
Figure 2.8: Sinusoidal modulation of temperature used in modulated differential scanning calorimetry.[17]

The equation governing sinusoidal oscillations used in MDSC are given by Equation 2.2

$$T = T_0 + \beta t + A_T \sin(\omega t) \tag{2.2}$$

where T and T_0 are the temperatures of the sample at time t and $t = 0$, A_T and ω are the amplitude and frequency of the perturbation, and β is the heating rate [18]. The benefit of MDSC is that by separating the sine wave in to its real and imaginary components, the reversible and nonreversible components of the heat capacity and heat flow can be found. The terms "reversible" and "nonreversible" may be a bit misleading, as they do not refer to the reversibility or nonreversibility of a phase transition. The purpose is rather to separate the total heat flow into the part of the specific heat that responds to heating rate and the part that responds to absolute temperature [19]. The ability to analyze these parts separately can be useful for studying glass transitions, first-order phase transitions, and overlapping phenomena [18].

2.4 Microscopy

2.4.1 Cross-Polarizing Microscopy

Polarized light is randomly oriented light that has been filtered such that the remaining light waves all oscillate in the same plane [20]. In cross-polarizing microscopy, light passes through a first polarizing filter, and is then blocked by a second filter oriented at a right angle to the first. Polarizing microscopes use polarized light to enhance the contrast of images obtained with birefringent (doubly refracting) materials [21]. The light from the source passes through a polarizer before passing through the birefringent specimen, and then is passed through a second polarizer, known as an analyzer, which recombines the light rays, as shown in Figure 2.9.
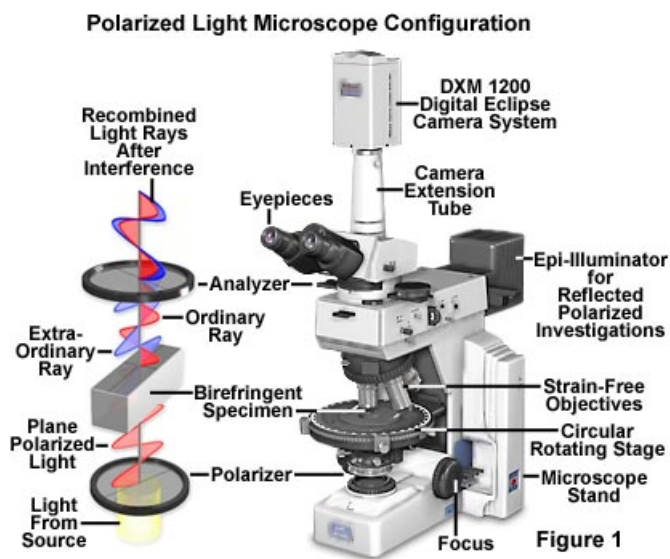
Figure 2.9: A diagram of a cross-polarizing microscope[21].

The contrast in the image occurs when the birefringent specimen produces two wave components of different velocities that, when recombine, interfere constructively and destructively. The contrast-enhancing properties of polarizing microscopy can provide detailed information about the structure and composition of materials.

2.4.2 Fluorescent Microscopy

Some substances have the ability to absorb and then re-emit light, which is known as fluorescence [22]. This process occurs almost instantaneously, however, when the emission remains after the excitation light has been removed, this is known as phosphorescence. The wavelength of the emitted light is always at a longer wavelength than excitation wavelength. Fluorescence microscopy is often used in biological research, as many samples can be stained with a dye that will fluoresce, allowing to identify cellular components that have been stained among those which have not. Figure 2.10 shows a modern epi-fluorescence microscope. For a microscope to be considered epi-fluorescent, the light from the excitation source and the detection of the fluorescence are done through the same light path.
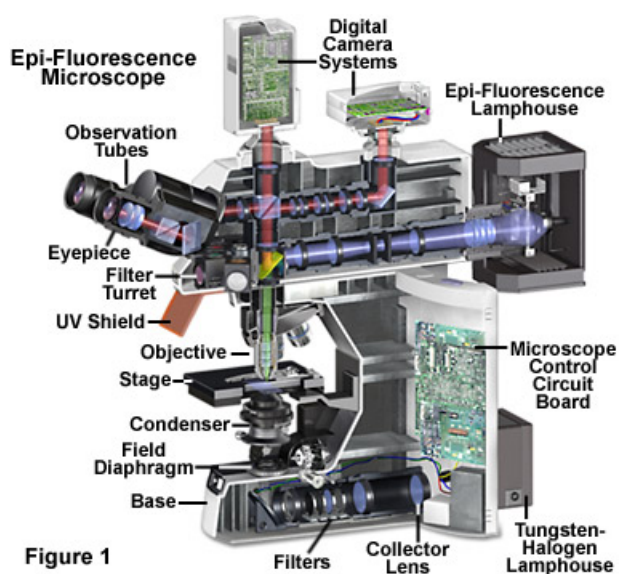
Figure 2.10: A diagram of an epi-fluorescence microscope[22].

2.4.3 Phase Contrast Microscopy

Phase contrast microscopy is an optical technique that enhances the contrast of transparent specimens [23]. It does this by translating small differences in phase to a change in amplitude that is seen as a difference in image contrast. This technique is often used for biological samples and the advantage is that living cells do not need to be stained to be visualized. A

diagram of a phase contrast microscope can be seen in Figure 2.11.
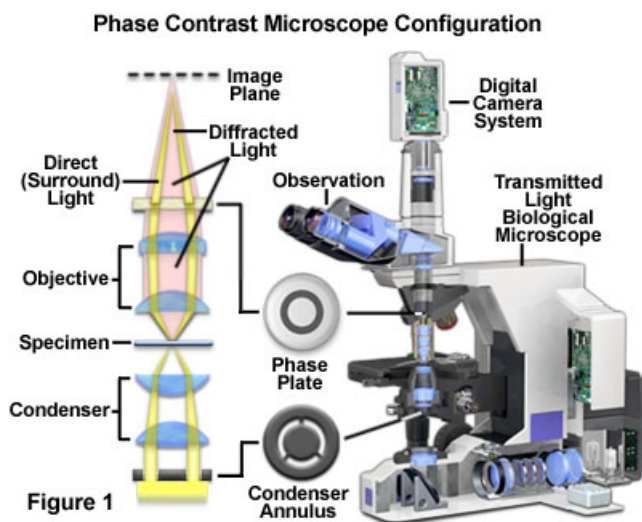
Figure 2.11: A diagram of a phase contrast microscope[23].

3 Methods

3.1 Vesicle-LC Mixture Preparation

Lipid vesicles are often used as "model" cell membranes in biological research. To create these lipid vesicles, I used 2- Oleoyl-1-palmitoyl-sn-glycero-3-phosphocholine (POPC), obtained from Sigma-Aldrich (refer to Appendix A for full description of materials). POPC is a lipid that occurs naturally in eukaryotic cell membranes, and is an appropriate substitute that will mimic many properties of a human cell.

3.1.1 Creating Lipid-LC Solution

The first step in the process is to disperse the lipid in a solution of solvents. The solvents used are chloroform and methanol in a 2:1 vol:vol solution. A ratio of 2mg of POPC to 1 mL of solvent to solution was found to work well for these experiments. Secondly, two different amounts of 3,3'-Dihexyloxacarbocyanine iodide (diI) were added. A ratio of 10 mg/mL in initial experiments and 1 mg/mL for all quantitative data collection experiments was used. diI is a fluorescent lipid dye that allows for clear imaging of the vesicles under fluorescent conditions. The different concentrations of diI lead to various effects, explained later. Third, 5CB liquid crystal was added to this solution by volume fraction. 5CB is in a liquid phase at room temperature, so a digital pipette was used to make accurate measurements of the liquid crystal.

3.1.2 Sample Preparation

The samples were prepared on microscope slides and in DSC pans. Further preparation details are provided in their respectful sections, however, a similar procedure is used in each case. A drop of the lipid solution is placed on the slide and the solvents are allowed to evaporate at room temperature. Then deionized water is added, allowing the vesicles to self-assemble.

3.2 Measuring Vesicle Size as a Function of 5CB Concentration

To study the influence of the liquid crystal on the formation of vesicles, samples at various concentrations were created and images of the vesicles gathered to see if the size of the vesicles was concentration-dependent. Following the vesicle-LC mixture preparation described above, samples at 0, 1, 2, 4, 6, and 8% by volume 5CB were created. All other chemicals were held constant at values mentioned previously.

3.2.1 Slide Preparation

Each slide for this experiment was prepared the same way. The glass vial with the lipid solution was shaken for 30 seconds. Then a 10 μL drop of the solution was placed on a clean glass slide. After letting the solvents evaporate at room temperature, the sample was rehydrated with a 10 μL drop of deionized water. Five slides were prepared for each concentration.

3.2.2 Imaging Procedure

The microscope used for this imaging procedure was a Nikon Eclipse TE300 inverted phase contrast microscope. This microscope has a long working distance, allowing observation of thicker specimens, and has a high UV transmission rate [24]. An image of the microscope can be seen in Figure 3.1.
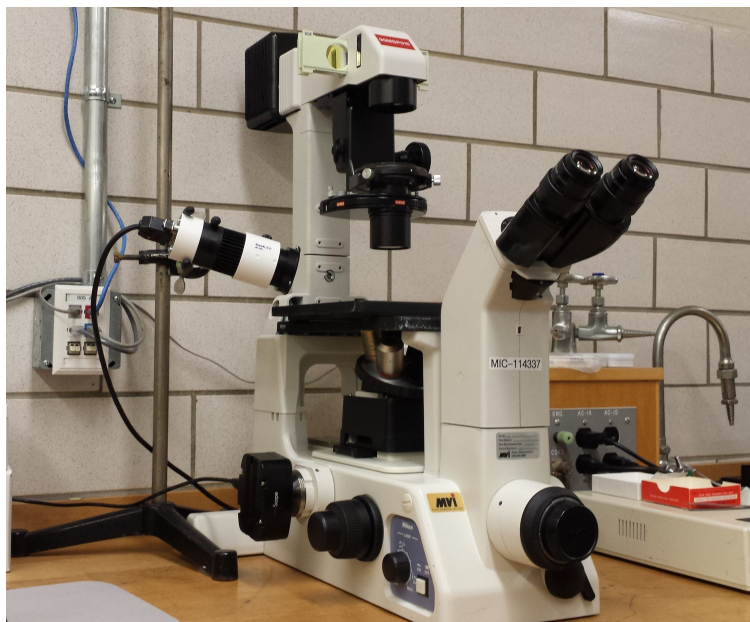
Figure 3.1: An image of a Nikon Eclipse TE300 inverted phase contrast microscope.

The camera used on this microscope was an AmScope MA1000 digital camera. It is a 10 megapixel camera with a pixel size of 1.67 x 1.67 μm [25].

Because of the large size of the vesicles, all images were taken at 4x magnification. For each slide, five images were gathered, attempting to capture different areas of the slide with each image. The largest vesicles filled most of the field of view, so a sampling bias was introduced. A choice of how many images of large vesicles had to be made, as images with partial vesicles will not be accounted for by the image analysis procedure. An attempt was made to take a consistent distribution of images containing large vesicles and smaller vesicles.

3.2.3 ImageJ Analysis

The analysis was automated using ImageJ. ImageJ is an open source image processing program developed by the National Institutes of Health [26]. One of the most powerful features of ImageJ is the ability to record macros and run batch analysis. By using the "Record" feature, it is possible to easily convert manual actions to script which can be automated. The script used ran a feature of ImageJ that would automatically adjust the threshold of

the image so that the edges of the dark vesicles could be found, and the contained area recorded. Refer to Appendix B for the script used. Figure 3.2 shows a comparison of an image collected with its mask drawing.
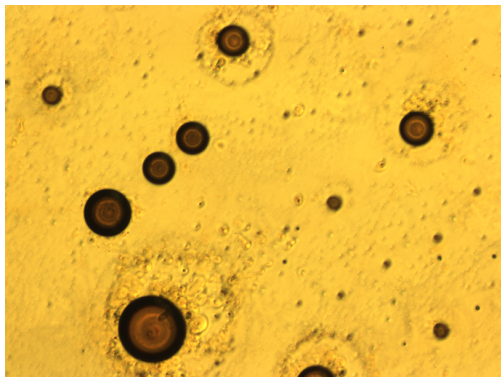
(a) 6% 5CB, phase contrast microscope, 4x
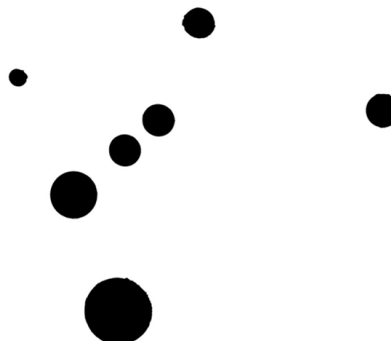
(b) Mask drawing of image

Figure 3.2: A comparison of an image gathered on the phase contrast microscope and mask drawing made using an automated ImageJ macro.

3.3 Observing Evolution of the System Using Microscopy

Because 5CB is birefringent on a cross-polarizing microscope when in the nematic phase, the nematic to isotropic phase transition can be easily seen when the image darkens. Using a temperature controlled hot plate and the time-lapse feature on microscope camera, the birefringence of 5CB-lipid mixtures could be measured and plotted as a function of temperature.

3.3.1 Slide Preparation

Because drying has a significant effect on the vesicle samples, the slides had to remain hydrated throughout data collection. To accomplish this, a well on the slide was constructed using 250 μm thick plastic. The plastic was adhered to the slide using quick-drying two part epoxy. An example of a cell can be seen in Figure 3.3.
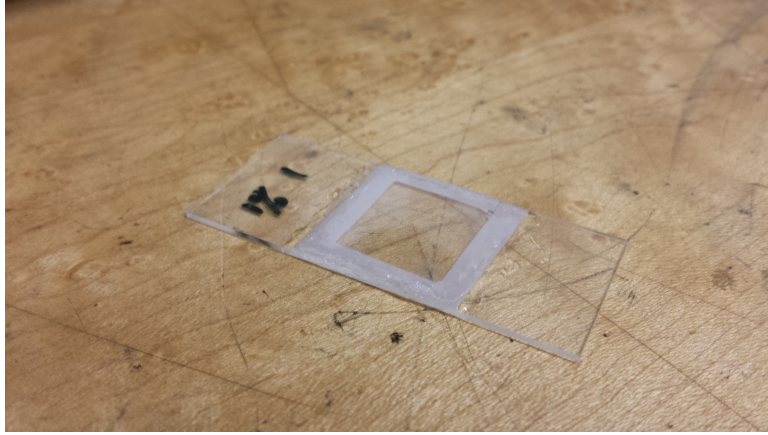
Figure 3.3: An example of a microscope slide cell.

As before, a drop of the lipid-LC solution was placed on the glass slide and allowed to dry. Then the cell was filled with deionized water and a cover slip was sealed on. The first attempt to seal the cover slip was with acrylic nail-polish, however, the acetone vapors given off by the nail polish seemed to destroy the samples. A two-part quick drying epoxy was used instead, as these types of epoxy do not give off vapors and only react with itself.

3.3.2 Experimental Setup

The cross-polarized microscope used in this experiment was a circa 1970 Labolux-pol Leitz Wetzlar microscope [27], as can bee seen in Figure 3.4. The camera used on this microscope was an AmScope MU300 digital camera. This camera has a resolution of 3 megapixels and a pixel size of 3.20 x 3.20 μm [28].

Figure 3.4: An image of a circa 1970 Labolux-pol Leitz Wetzlar microscope.

The slide was placed on the hotplate and covered with a metal plate, allowing for uniform heating. A black cloth was used to surround the microscope stage, reducing the parasitic light. Using the ToupView software provided with the microscope camera, time lapse images were taken every 30 seconds. When the camera began taking images, the temperature of the hot plate was ramped by 0.2 °C per minute.

The temperature controller used to control the hot-plate was a LakeShore 340 Temperature Controller. This temperature controller is designed to control samples under cryogenic bath situations [29]. Because these experiments were conducted without a large thermal bath, the hot-plate temperature did not scale at the exact rate set by the controller. Although the hotplate did not scale exactly at 0.2 °C per minute, it did scale at a constant rate. Each image correlated to a change of approximately 0.91 ± 0.03 °C. Using this procedure, the image number could be correlated to the temperature of the hotplate. The images could then be used to study the phase transitions of the liquid crystal.

3.3.3 Image Analysis

The data collected from the images was done using the batch measuring feature in ImageJ. Using this procedure, the total and mean intensity of an entire image or region of interest was found. The batch processing feature allows for rapid data collection on entire folders of images. The results were imported in the form of a spreadsheet to OriginPro. OriginPro is a powerful data analysis and scientific graphing software.

3.4 Differential Scanning Calorimetry

The calorimeter used in these experiments was a Model Q200 Modulated Differential Scanning Calorimetry (MDSC) machine from TA Instruments, use. Prior to the set of experiments conducted, the machine was serviced by TA instruments and calibrated using a sapphire disc. All pans used in this experiment were TA Tzero Pans and were sealed with TA Tzero Hermetic lids. An image of the calorimeter used can be seen in Figure 3.5.

Figure 3.5: An image of the Q200 model Modulated Differential Scanning Calorimetry machine from TA Instruments.

For my initial attempts with the MDSC machine, the lipid-LC solution was placed directly in the DSC pans. The vesicles did not self-assemble in the pans, as the material seemed to stick to the corners of the pan. As an alternative method, vesicles were created on a glass slide, rehydrated, and scraped into the DSC pan using a metal applicator. Then more water

was added to the sample.

Once the sample was created, and a cover was crimped on the pan, the sample was massed, and placed in the DSC machine along with an empty reference pan. The temperature was scaled at a rate of 1 °C per minute and 0.2 °C per minute from 20 to 45 °C and back down. This cycle was repeated twice for each sample.

When the data was analyzed, the heating and cooling runs were separated and the transience (large spikes seen while the machine equilibrates) were removed. Each plot of heat capacity was scaled by the sample mass to find the specific heat. Next, a straight line connecting the ends of each graph was subtracted. Although not a perfect model, the straight line approximates the contribution to the sample of the water. Thus any change in specific heat remaining is due to contributions from the liquid crystal, lipid, dye, or any other energetics of the system occurring.

4 Results and Discussion

4.1 Vesicle Formation

For a previous experiment, vesicles were created using the same procedure as described above, however, without the addition of liquid crystals. The best vesicles found using this procure are shown in Figure 4.1
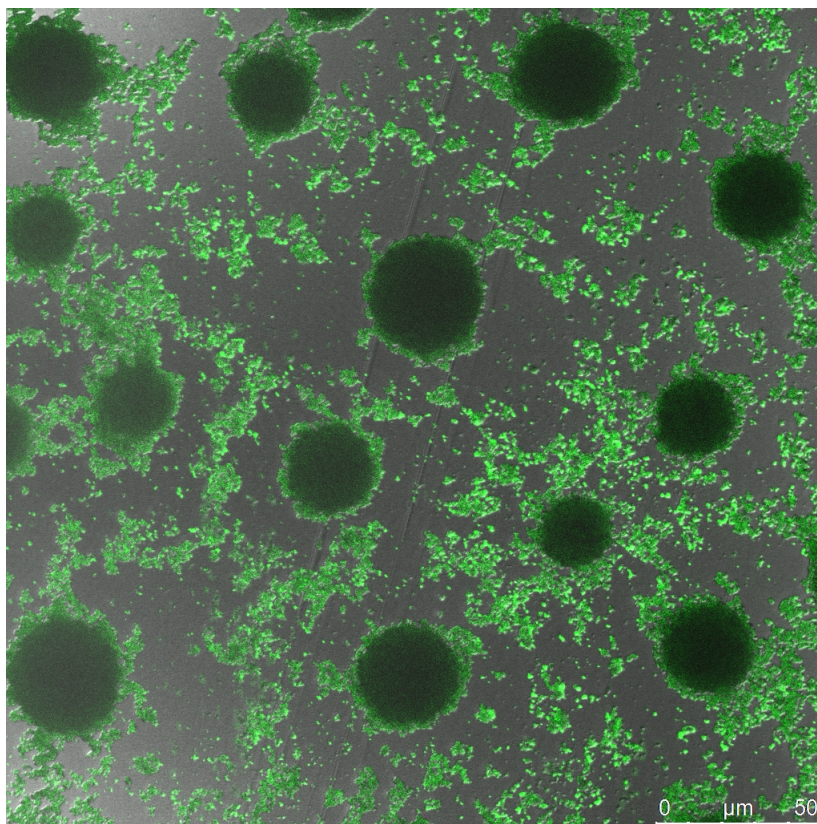
Figure 4.1: Vesicles created without liquid crystal, imaged on Leica epi-fluorescent confocal microscope.

As the figure shows, the vesicles were not well formed, having rough surfaces and being on the order of 20-40 μm.The addition of liquid crystals had a significant impact on the formation of the lipid vesicles.

The most notable aspect of the lipid-liquid crystal mixture was that when the solvents evaporated, extremely large vesicles formed. In fact, they are so large many of them can be seen with the naked eye. An example of typical lipid structures can be seen in Figure 4.2.
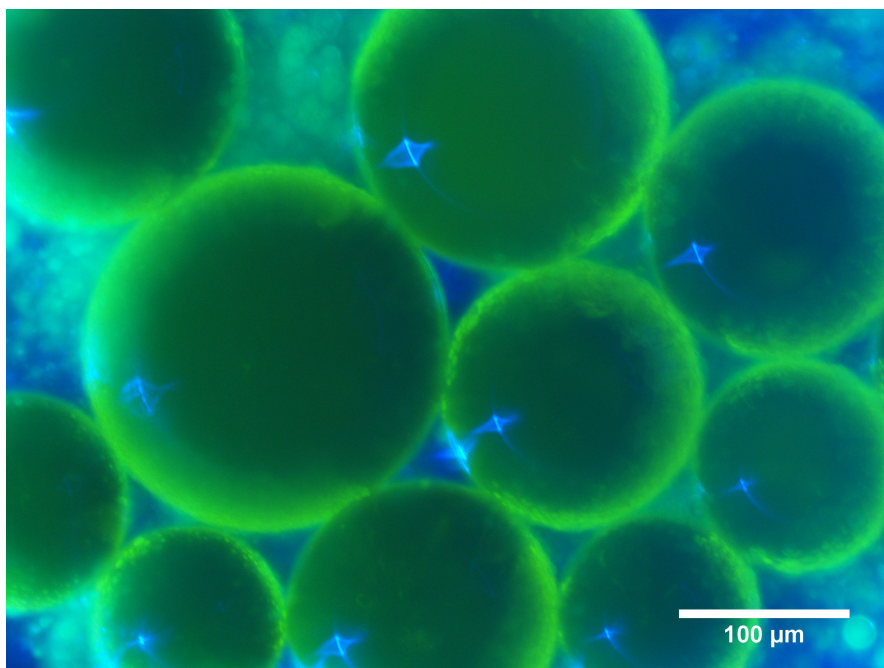
Figure 4.2: Typical lipid vesicle structures formed in the presence of 5CB liquid crystal, imaged on a Nikon MM40 surface scan scope under fluorescent conditions.

As the image shows, the vesicles created are much larger than formed in the absence of liquid crystal. The blue arcs seen inside the vesicles are caused by the blue fluorescent light being focused by the vesicles. This lensing effect demonstrates the nearly spherical nature of the vesicles.

To understand the role of the liquid crystal, samples containing 5CB and 10CB were compared. These two liquid crystals are nearly identical, as they both phase separate in to oily droplets in water. However, 5CB is in the nematic phase at room temperature and 10CB is in the smectic phase. Figure 4.3 shows the difference between two samples prepared with the different liquid crystals under otherwise identical conditions. The nematic phase of 5CB allows for radially ordered droplets of liquid crystal to form, as indicated by the cross patterns seen on a cross-polarized microscope. The 10CB, however, does not have radial ordering, and thus does not allow vesicles to form. The ordered structures seen on a cross-polarized microscope are just smectic domains.

(a) 2% 5CB, 24°C, 10x　　　　　　　　(b) 2% 10CB, 24°C, 10x
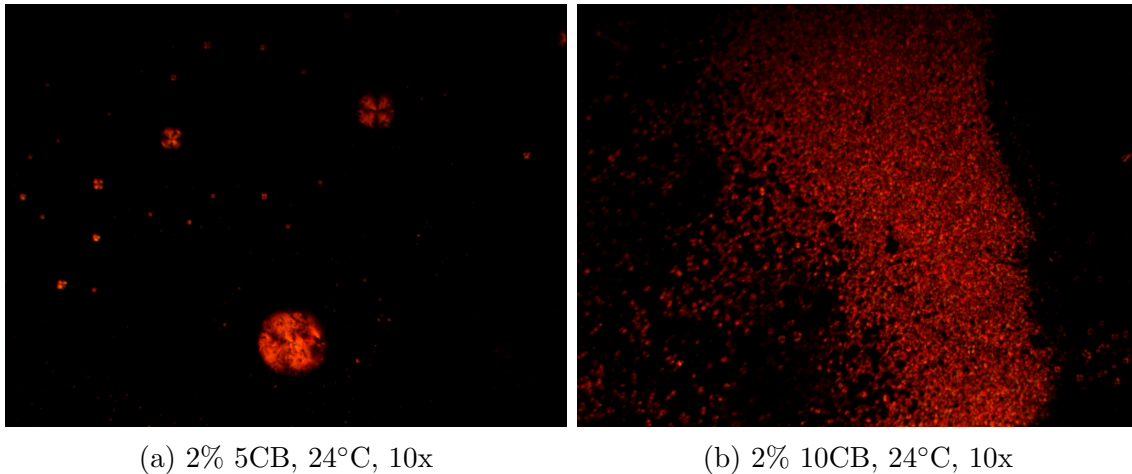
Figure 4.3: A comparison of identical lipid samples containing 5CB and 10CB at room temperature, imaged with a cross-polarized microscope.

4.2 Vesicle Size 5CB Concentration Dependence

To understand the effect of the liquid crystal on the size of the vesicles, series of images of samples with different concentrations of 5CB were gathered and analyzed in order to determine the size of the vesicles. The analysis showed the average size of the vesicles increased with increasing concentration of 5CB. However, the large standard deviation indicated a non-Gaussian distribution, which proved to be interesting.

Using the ImageJ macro found in Appendix B, the mean vesicle diameter and standard deviation for each concentration was determined. The results of which can be seen in Figure 4.4
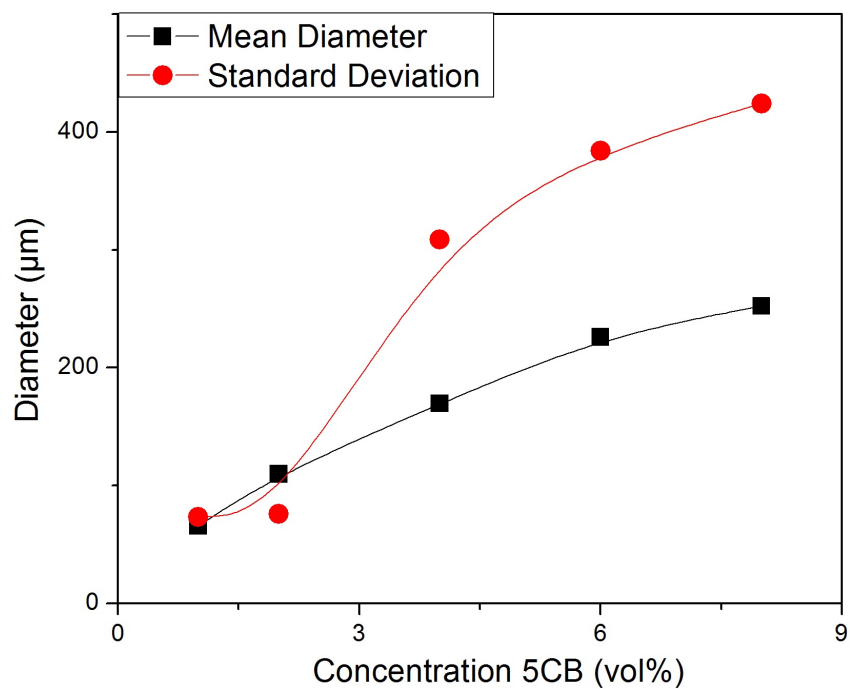
Figure 4.4: The mean vesicle diameter plotted as a function of concentration 5CB.

Figure 4.4 shows the standard deviation is extremely large, and in most cases is larger than the mean diameter. To understand what was causing the standard deviation to be so large, histogram plots were created to show the distribution of the vesicle sizes. Bin sizes of 30 μm were used for each plot and the smallest vesicles found were approximately 30 μm in diameter. The results of the vesicle distributions at each concentration can be seen in Figures 4.5-4.9.
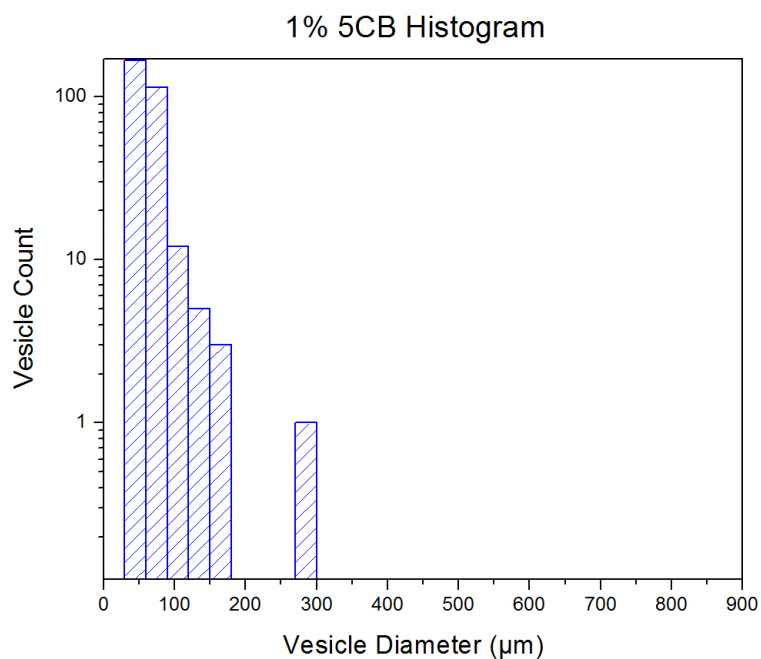
Figure 4.5: A vesicle distribution histogram for 1% 5CB at room temperature.
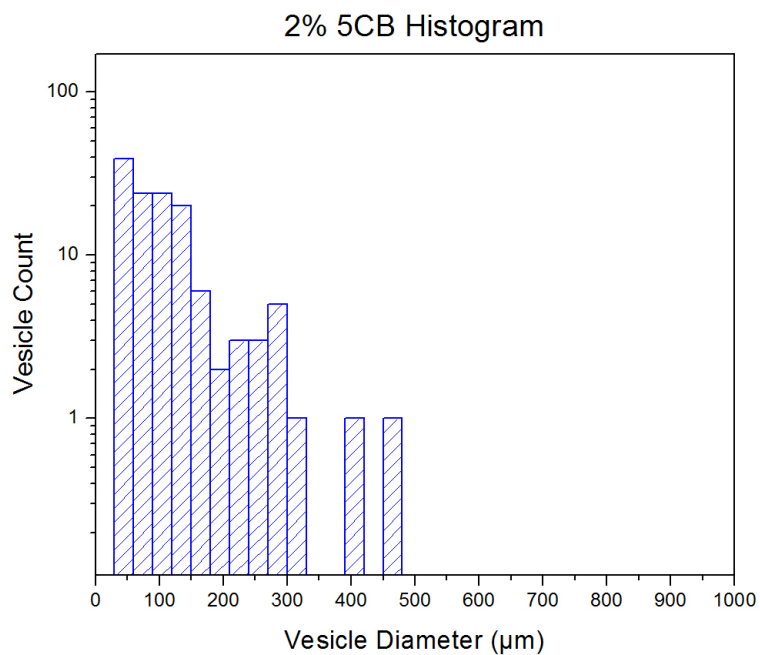
Figure 4.6: A vesicle distribution histogram for 2% 5CB at room temperature.
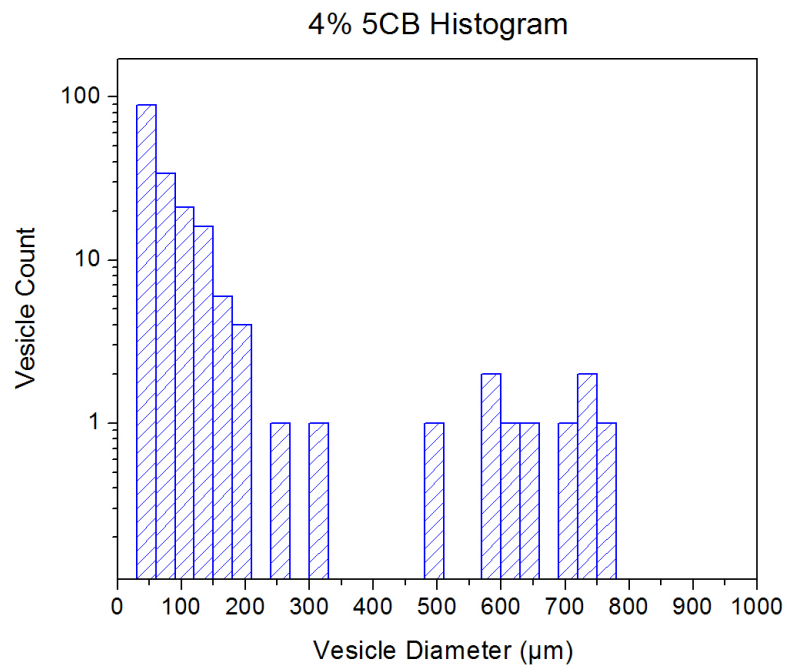
Figure 4.7: A vesicle distribution histogram for 4% 5CB at room temperature.
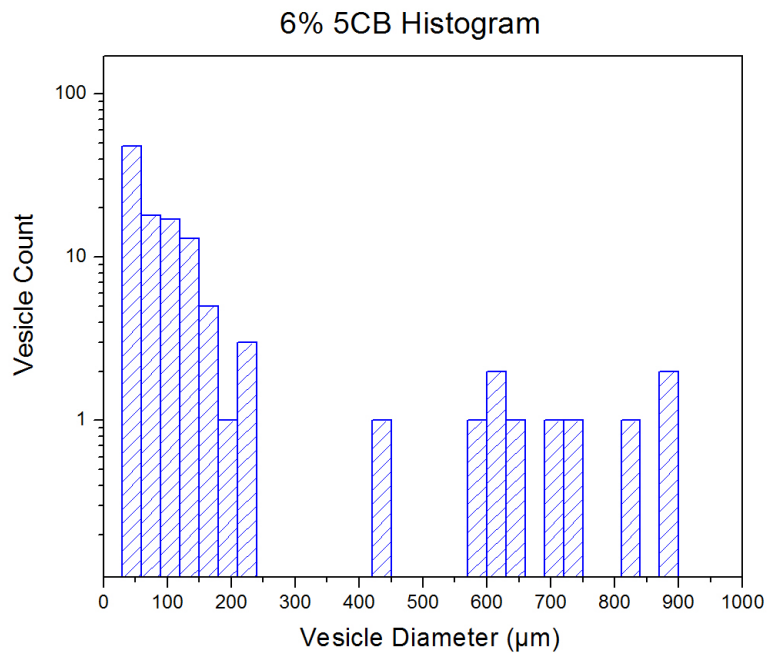
Figure 4.8: A vesicle distribution histogram for 6% 5CB at room temperature.
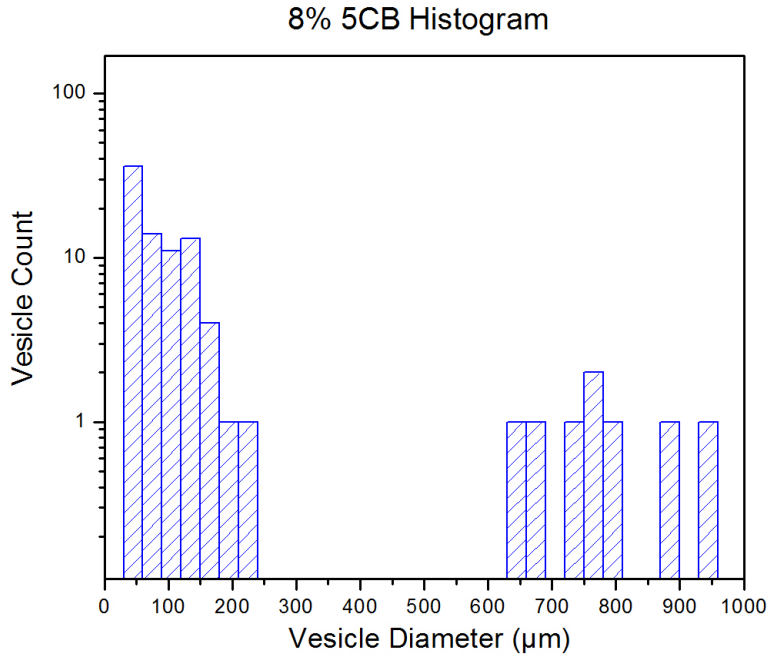
Figure 4.9: A vesicle distribution histogram for 8% 5CB at room temperature.

As the histograms show, the distribution is non-Gaussian, which explains why the standard deviation in Figure 4.4 was so large. Additionally, it appears that the distribution is bimodal, having collections of many small vesicles with several larger vesicles. In each histogram, a gap appears to separate the small and large vesicles. The distribution was split into two sections, before and after the gap. The gaps in each distribution are given in Table 4.1. Using both groups of vesicles, new calculations were performed for the mean and standard deviation. These results are presented in Figure 4.10.

Concentration 5CB	Gap Range
1%	160-276 μm
2%	310-393 μm
4%	302-497 μm
6%	230-434 μm
8%	228-642 μm

Table 4.1: A table of gap sizes separating the small and large vesicle groups in distribution histograms.
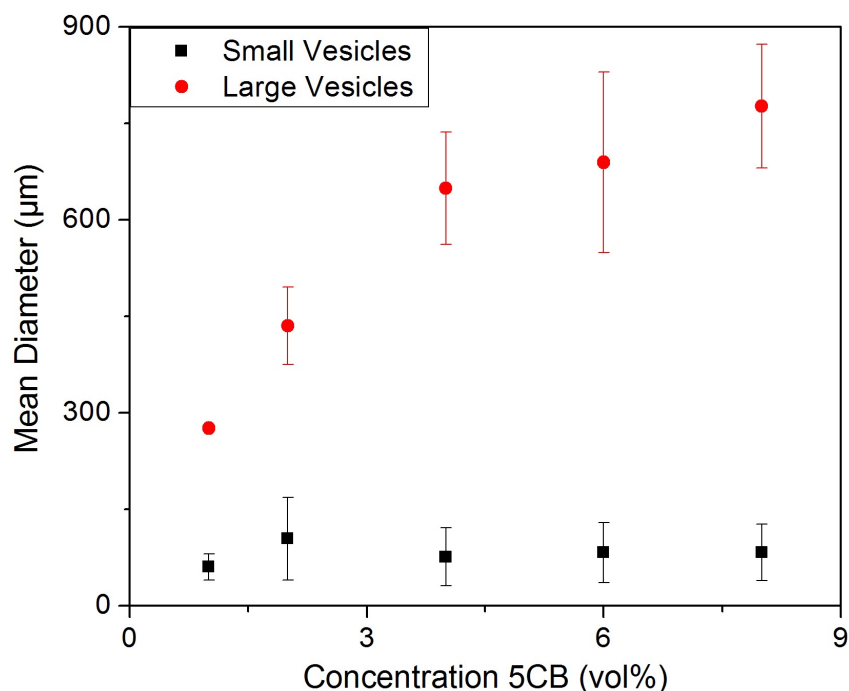
Figure 4.10: Bimodal means of vesicle sizes as a function of concentration-here error bars represent standard deviation for each sub-group.

It seems that a bimodal description of the system is accurate, as the standard deviations are much smaller. For each concentration of 5CB, the mean diameter of the smaller vesicles remained between 70-100 μm and the mean diameter of the larger vesicles grew with concentration. What this possibly means is that the small vesicles self-assemble at a nearly constant size when in solution. The larger vesicles form when the droplet phase separates as it is drying.

4.3 Phase Transitions Studied with Cross-Polarizing Microscopy

Birefringent materials are substances which can uniformly rotate the polarization of light. These materials can then be seen on a cross-polarized microscope as they appear as bright spots when looked at through an analyzer. For this reason, cross-polarized microscopy is often used in the study of liquid crystals. In the nematic phase or smectic phase, liquid crystals will be birefringent, however, in the isotropic phase the image will be dark. This

property can be used to study the phase transitions by analyzing the intensity of light in an image gathered on a cross-polarized microscope. The image gathering and analysis procedure described in Section 3.2 was used to gather phase transition behavior of samples containing various concentrations of 5CB. Figures 4.11-4.15 show mean intensities of each image gathered for the various concentrations.
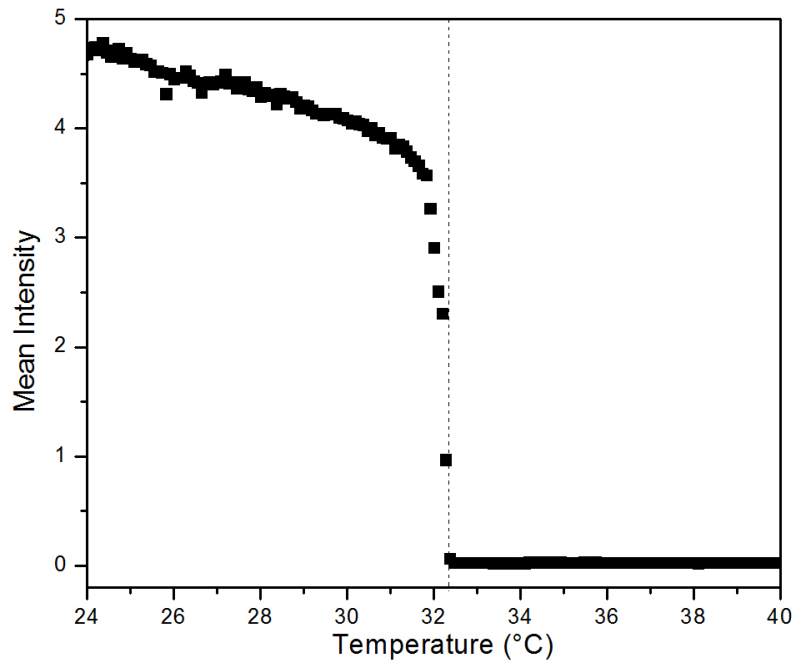
Figure 4.11: The total mean intensity as a function of temperature for 1% 5CB.
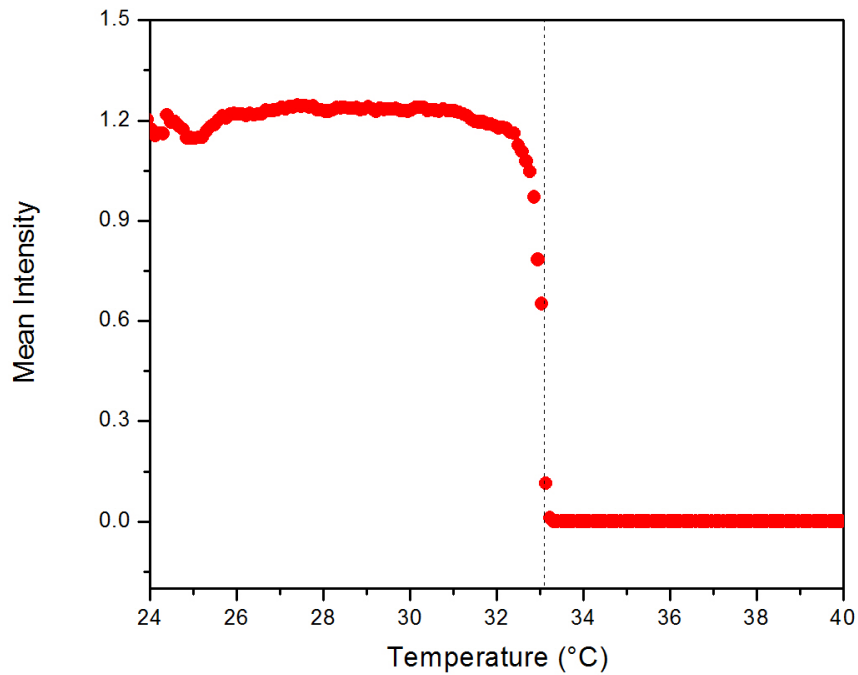
Figure 4.12: The total mean intensity as a function of temperature for 2% 5CB.
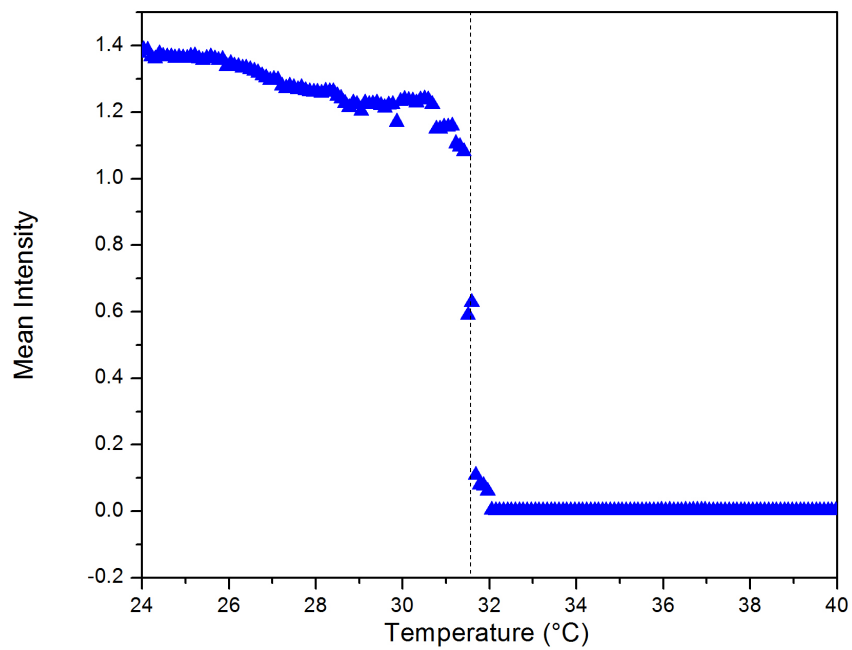
Figure 4.13: The total mean intensity as a function of temperature for 4% 5CB.
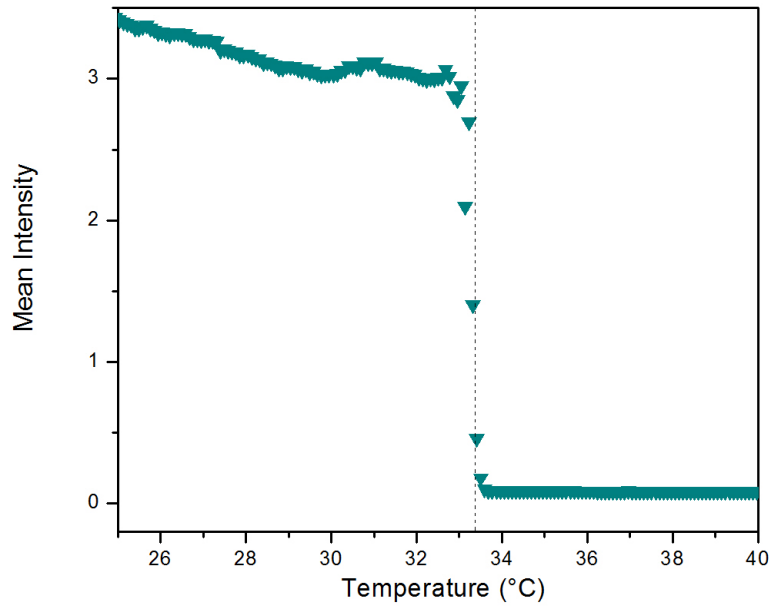
Figure 4.14: The total mean intensity as a function of temperature for 6% 5CB.
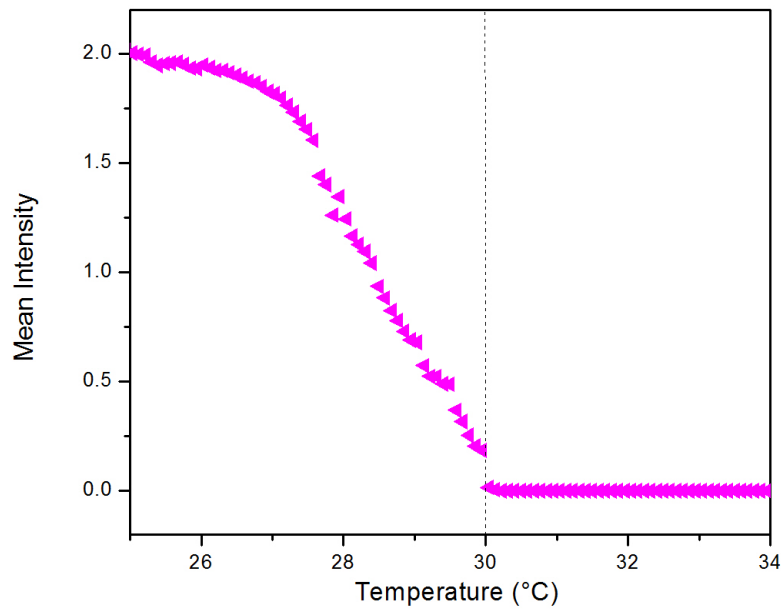
Figure 4.15: The total mean intensity as a function of temperature for 8% 5CB. Note the abnormally slow decrease in intensity leading to the phase transition.

As this analysis demonstrates, the phase transition of the liquid crystal can be clearly seen where the intensity drops rapidly. Also, the transition temperatures of each sample range between 30 and 34 °C. This is consistent with experiments with 5CB found in the literature. The bulk transition temperature of 5CB is 35 °C, and as impurities are added the transition temperature is lowered. Numerical values of the total transition temperatures can be found in Table 4.2.

Concentration 5CB	Transition Temperature (°C)
1%	32.40 ± 0.10
2%	33.15 ± 0.10
4%	31.88 ± 0.10
6%	33.48 ± 0.10
8%	30.00 ± 0.10

Table 4.2: N-I phase transition temperatures found by cross-polarized microscopy and image analysis of total image areas.

The only sample that did not transition very rapidly was the 8% sample. For the sample, all parameters were maintained the same, except the glass cover slip was simply floated on top of the sample cell rather than sealed with epoxy. This may have caused the slow transition and lower transition temperature, however, there is not yet any evidence beyond that to support this hypothesis.

Although the analysis of the images gathered on the cross-polarized microscope have provided some general data about the phase transitions of the liquid crystal, the technique can be further improved upon to gather more information. As the images showed, not all of the 5CB droplets transitioned at the same temperature. By using the region of interest function in ImageJ, individual vesicles could be isolated and analyzed to find their transition temperature. The results of this procedure for one sample can be seen in Figure 4.16.
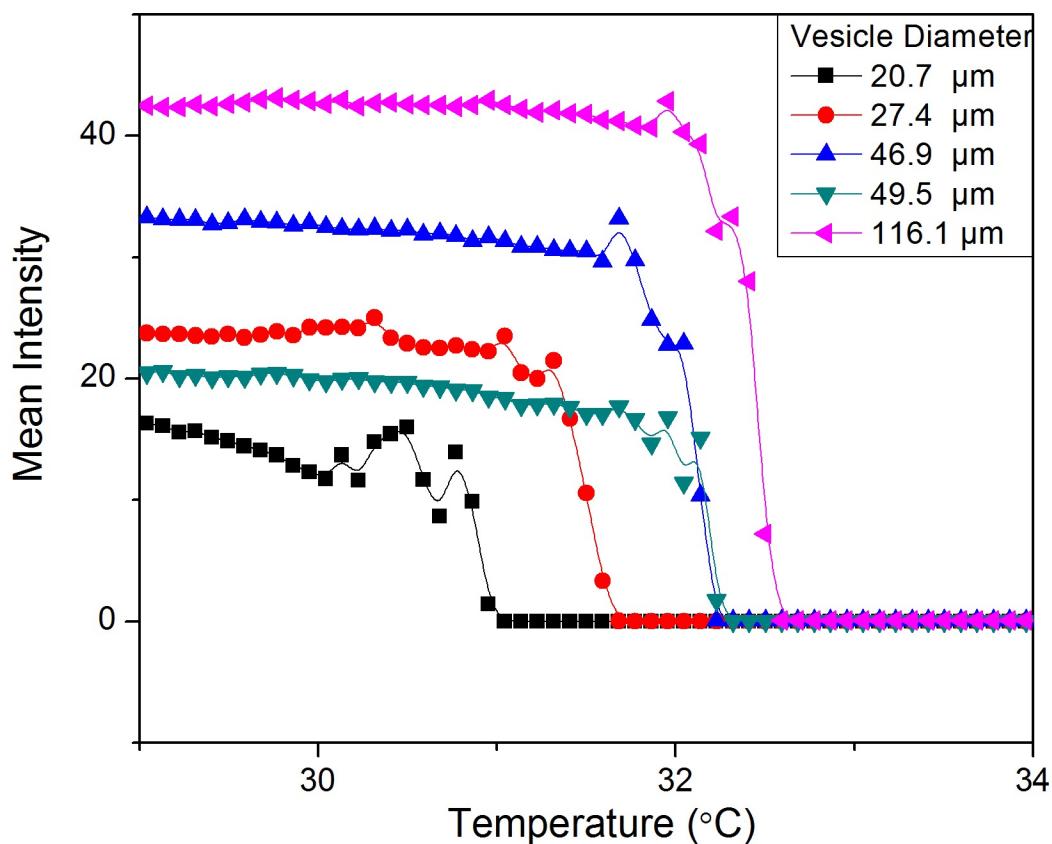
Figure 4.16: A heating scan at 0.2 °C/min for 1% 5CB demonstrating phase transitions for individual vesicles.

As Figure 4.16 shows, the vesicles transitioned at different temperatures spanning almost 2 °C. When analyzing an entire image, this resolution is lost, as any decrease in intensity vesicle phase transition will only show up in the analysis as a small decrease in overall mean intensity. By isolating individual regions, the size effects of the 5CB droplets can be studied. A plot of the phase transition temperatures as a function of vesicle size can be found in Figure 4.17.
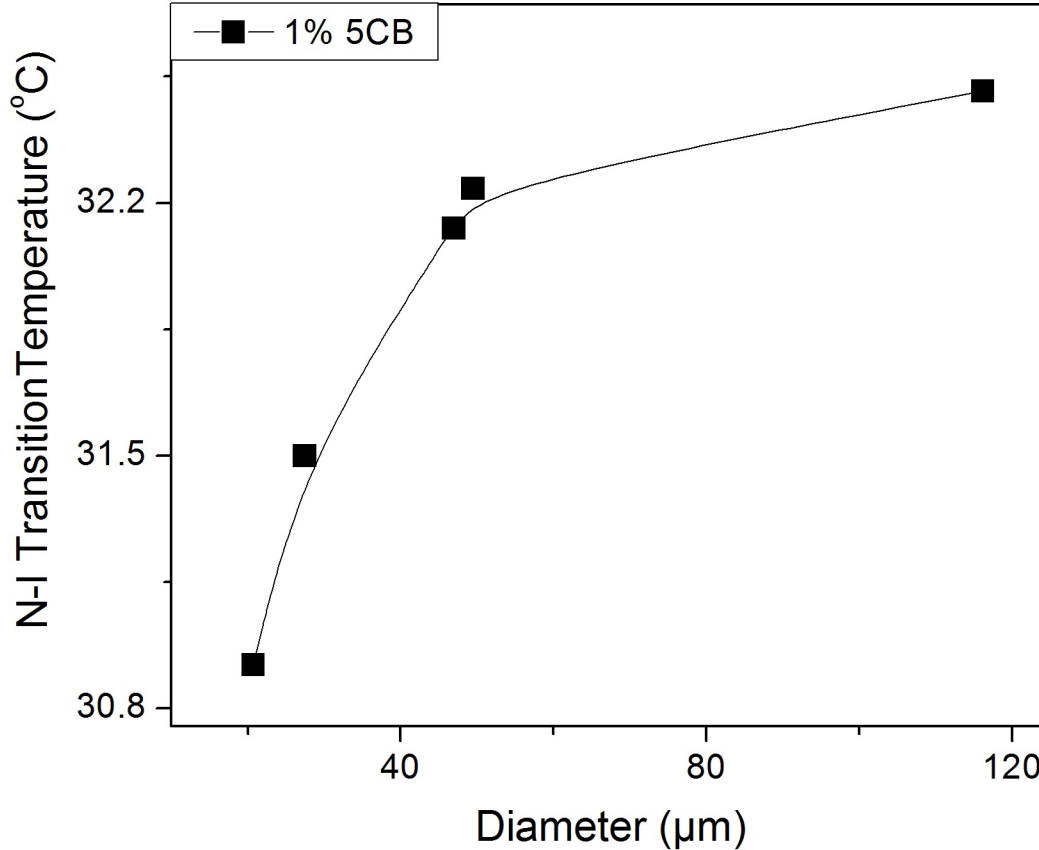
Figure 4.17: A comparison of the N-I phase transition temperatures for different diameter vesicles.

Figure 4.17 seems to demonstrate that as the vesicle diameter decreases, the transition temperature falls off rapidly. Also, it appears as if the transition temperature of larger vesicles plateaus several degrees below the bulk transition temperature of 5CB. This suggests water may be dissolved in the droplets of liquid crystal, or there is some sort of diffusion process occurring lowering the phase transition temperature.

Repeating the same procedure for heating trials run on other concentrations of 5CB, the phase transitions found by processing entire images can be more accurately analyzed. The results of which can be seen in Figure 4.18.
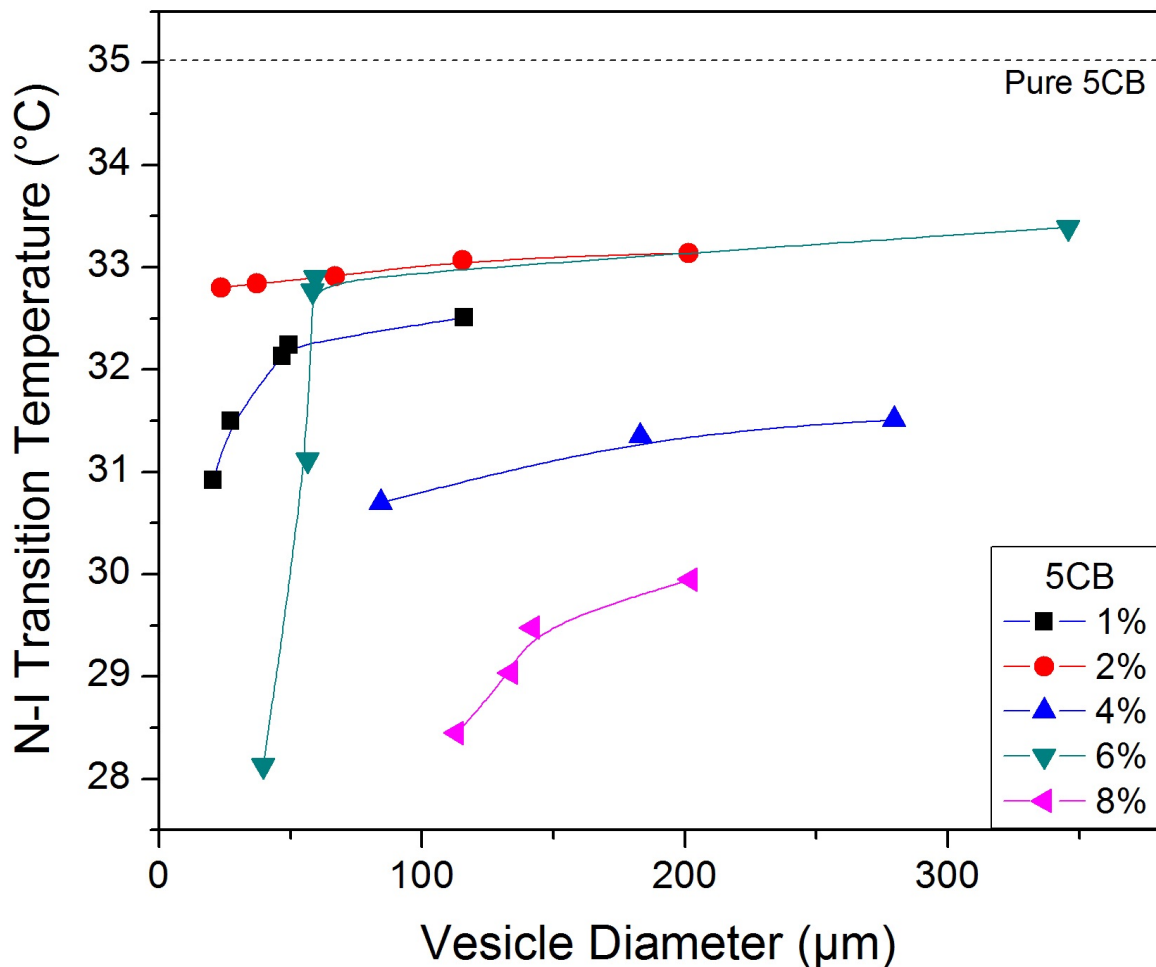
Figure 4.18: A heating scan at 0.2 °C/min showing the N-I phase transition temperatures for different diameter vesicles for samples containing varied 5CB concentrations.

If the size of the vesicle was the only parameter that effected the N-I transition temperature, the percent of the 5CB in the sample would not matter, and all points would collapse to a common curve. However, as Figure 4.18 shows, although the size seems to play a role in each sample, there is no common trend between samples. This indicates that there is some more complex factor altering the transition temperature of each sample. It could be possible there is some diffusion occurring that differs between samples. The preparation of the cells and sealing of the cover slips may also have an effect on the transition temperature. An interesting anomaly that occurred with several cells is described in Section 4.7.

4.4 Calorimetry Results

The results obtained from the calorimetry work includes reversible and non-reversible specific heat data for heating and cooling runs at two different scan rates. A rate of 0.2 °C/min was chosen to match the cross-polarized microscopy experiment, and a rate of 1 °C/min was chosen as most biological experiments are performed at that scan rate. Each sample was heated and cooled twice, however, the results presented only contain the second of these scans. This is due to the settling of the sample during the first heating run, which lead to some unreliable results.

The first comparison made with the data collected was an overlay of data from samples containing different concentrations of 5CB. By comparing the reversible and nonreversible specific heats for heating and cooling scans at different concentrations of 5CB, information can be gathered about the energetics of each sample. Please note that due to some data discrepancies, the 6% 5CB samples were omitted from the results. An example of one of the graphs created is shown in Figure 4.19. The remaining graphs can be found in Appendix C.
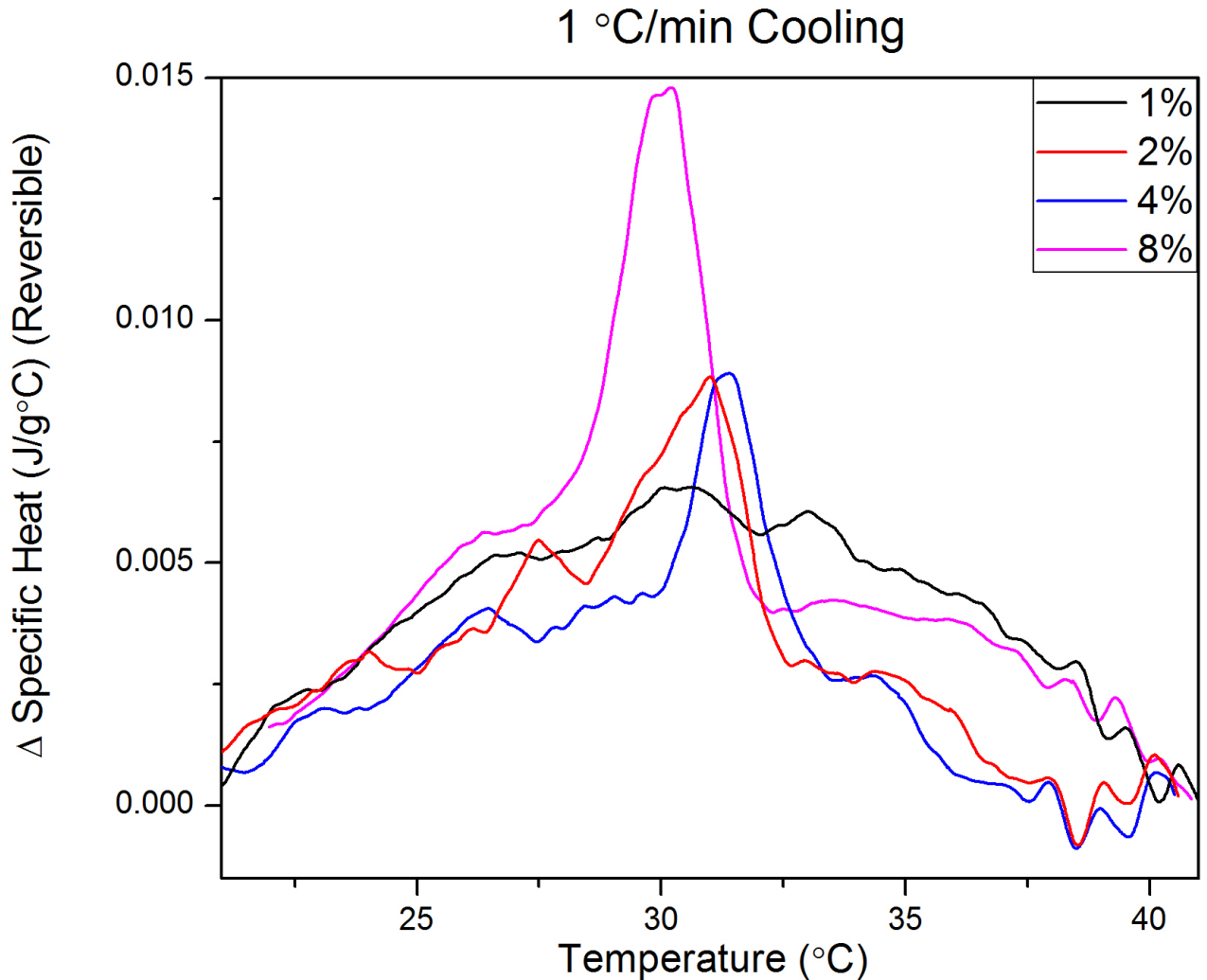
Figure 4.19: An overlay of reversible specific heat data for different concentrations of 5CB, with a 1 °C/min scan rate.

Figure 4.19 shows the reversible specific heat of a cooling run at a rate of 1 °C/min. The large spikes visible in the 2, 4, and 8% samples are likely indications of the N-I phase transition of the liquid crystal. If the liquid crystal was the only element of the system generating a heat signature, the remainder of the specific heat would be flat. However, all of the specific heats showed a curvature, indicating that there must be additional contributing energetics. The other features could be from the dye, water, lipid, or any interaction or restructuring of the sample. Because the system is so complex, it is difficult to determine what elements are responsible. Additionally, because different size droplets transition at

different temperatures, as discussed in Section 4.3, the broad spikes in specific heat could likely be composed of collections of smaller peaks from the individual phase transitions.

Similar to the experiment conducted with the cross-polarized microscope, it is worthwhile to compare the N-I phase transition temperatures between different concentrations of 5CB. The transition temperatures collected were found by calculating the midpoint of any large identifiable peaks in specific heat. Because not all trials contained clear phase transition signatures, some samples do not have a transition temperature reported. The results of this study can be found in Table 4.3.

%5CB	1 °C/min Heating	1 °C/min Cooling	0.2 °C/min Heating	0.2 °C/min Cooling
1	-	-	-	-
2	31.13 ± 0.05 °C	31.10 ± 0.05 °C	32.67 ± 0.05 °C	32.30 ± 0.05 °C
4	31.17 ± 0.05 °C	31.38 ± 0.05 °C	27.34 ± 0.05 °C	26.96 ± 0.05 °C
8	30.50 ± 0.05 °C	30.08 ± 0.05 °C	-	-

Table 4.3: The N-I phase transition temperatures found using MDSC.

The data found using calorimetry does not exactly correlate with the data found using the cross-polarized microscope. Additionally, there is some variance between transition temperatures found at different scan rates. Although minor differences between scan rates might be due to different response times of the liquid crystal, there is a large enough difference that indicates some other contributing factor. Likely the source of these discrepancies is the scraping procedure used to transfer the vesicles from the microscope slide to the test pan. It was difficult to get all of the material from the slide to the pan, so some large vesicles, or possibly many small vesicles, could have been left out of the sample. This would alter the overall transition temperature found by studying the total change in specific heat. Also, some of the vesicles could have burst in the transition process. This would again alter the transition temperature, and furthermore is impossible to repeat exactly the same way between trials.

Although the scraping procedure introduced large uncertainties, there is still more information that can be gathered from this experiment. In addition to plotting overlays of

specific heat for different concentrations of 5CB, individual heating and cooling runs can be analyzed. By creating hysteresis plots of heating and cooling trials, information about the evolution of the system can be obtained. An example of such a plot can be found in Figure 4.20
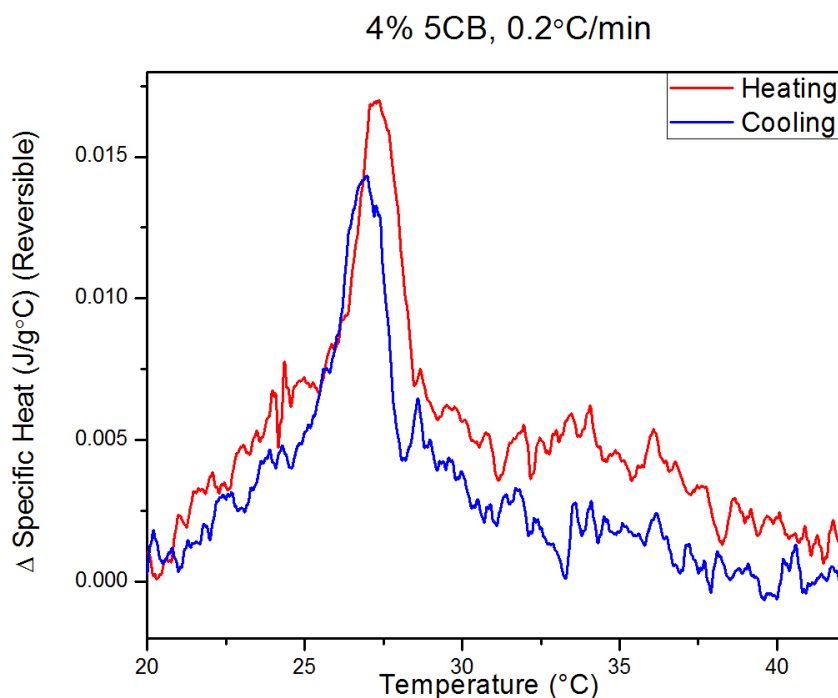
Figure 4.20: A hysteresis plot of reversible specific heat data for 4% 5CB at a 0.2 °C/min scan rate.

The remaining hysteresis plots are found in Appendix D. In nearly every hysteresis plot containing a clearly identifiable phase transition, the transition temperature is lower on the cooling scan than the heating scan. This could possibly occur as the amount of other chemicals dissolved in the 5CB increases over time by diffusion. This assumption would be consistent with the notion that diffusion is occurring, transporting materials in and out of the vesicles. Another possibility is that there is some sort of annealing process occurring when the sample is heated to 40 °C.

In addition to the hysteresis data, we can use the same plots to gather information about

the change in enthalpy of each sample. By integrating the specific heat over the entire temperature range, we can find the change in enthalpy. The results of this analysis can be seen in Figures 4.21-4.24.
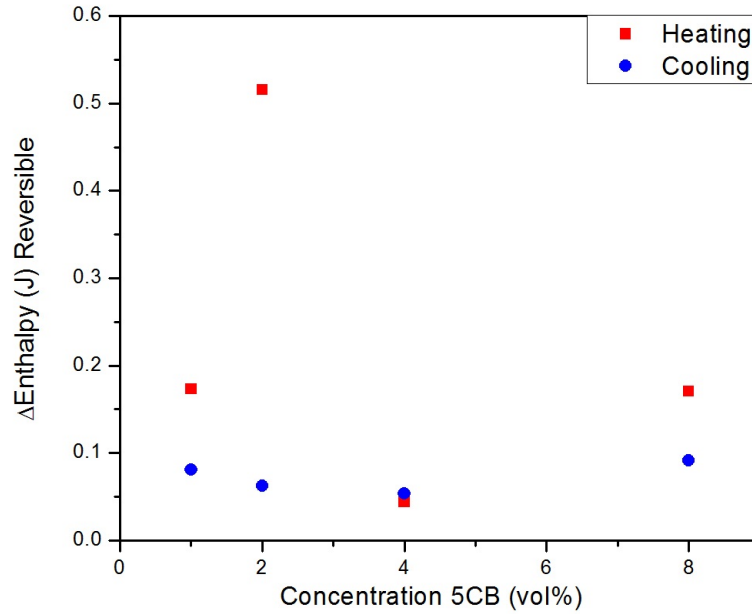
Figure 4.21: Change in reversible enthalpy data at 1 °C/min scan rate.
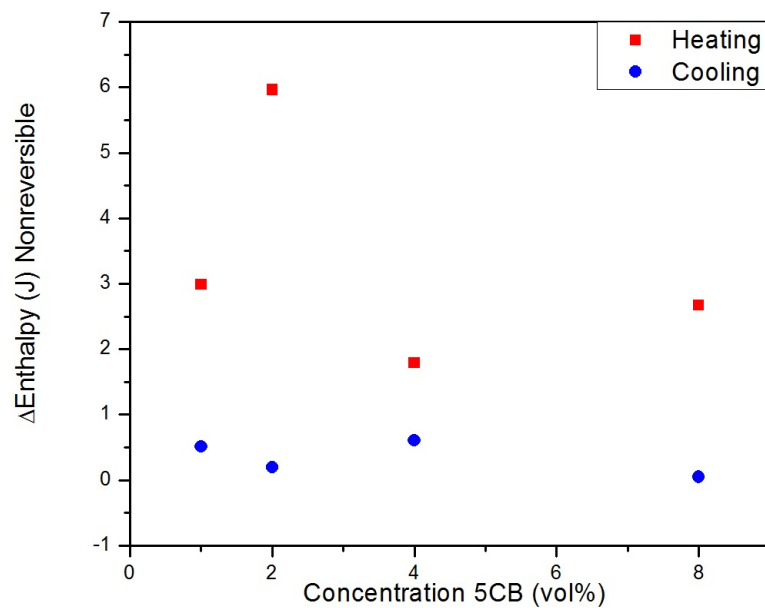
Figure 4.22: Change in nonreversible enthalpy data at 1 °C/min scan rate.
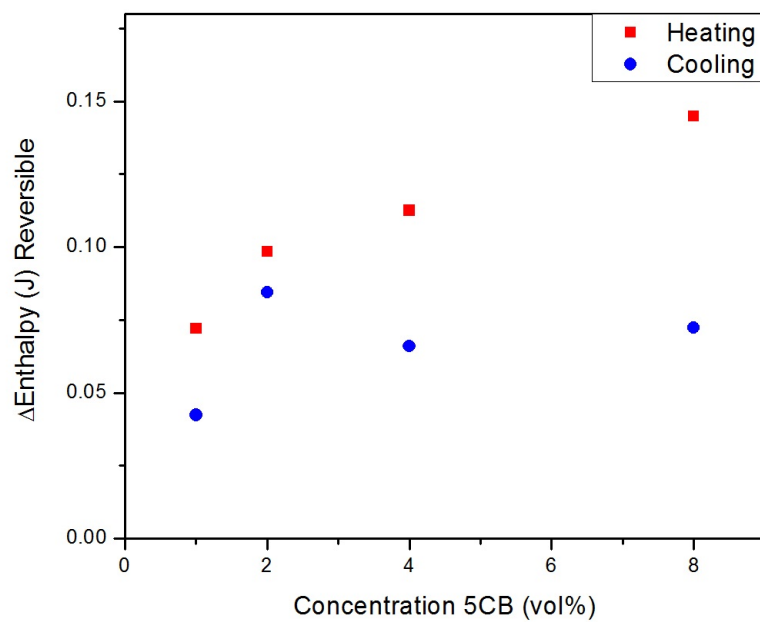
Figure 4.23: Change in reversible enthalpy data at 0.2 °C/min scan rate.
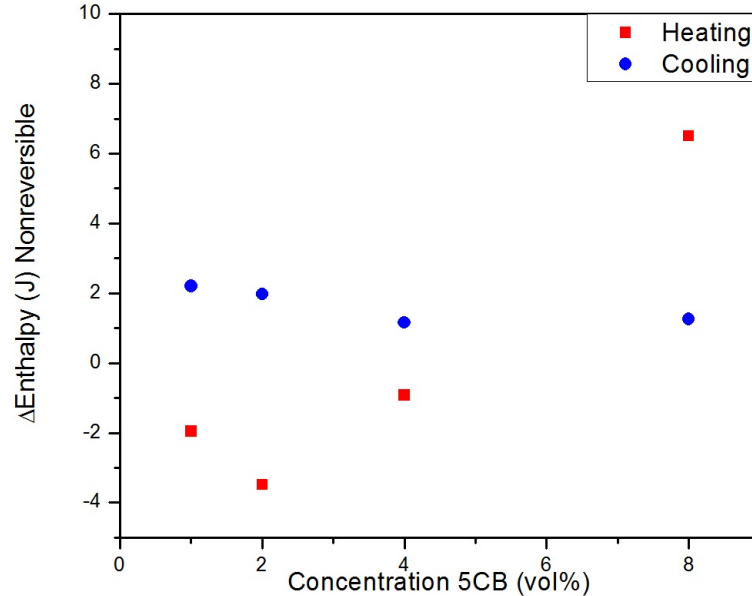
Figure 4.24: Change in nonreversible enthalpy data at 0.2 °C/min scan rate.

There are no apparent trends in the enthalpy data, however, much of the data is fairly flat. This indicates that although several samples contain peaks indicating a phase transition of the liquid crystal, the majority of the enthalpic change is due to other contributions from the system.

Although the data from the calorimetry work is not consistent, there are still some conclusions that can be drawn. For example, looking at the 2% sample, scanned at 0.2 °C/min, the N-I phase transition occurred at 32.67 °C. This transition temperature falls near the phase transition temperatures found for the 2% sample, as shown in Figure 4.18. By comparing this phase transition temperature to the 2% curve, it would appear as if the phase transition occurred at the temperature that the small vesicles transitioned at. It could be possible that the scraping procedure either did not capture any larger vesicles, or broke up the large vesicles in to smaller ones, which would transition at lower temperatures.

4.5 Dye Crystallization

In some initial tests, the samples were heated to 40 °C, and some birefringence could be seen on the cross-polarized microscope, as shown in Figure 4.25.
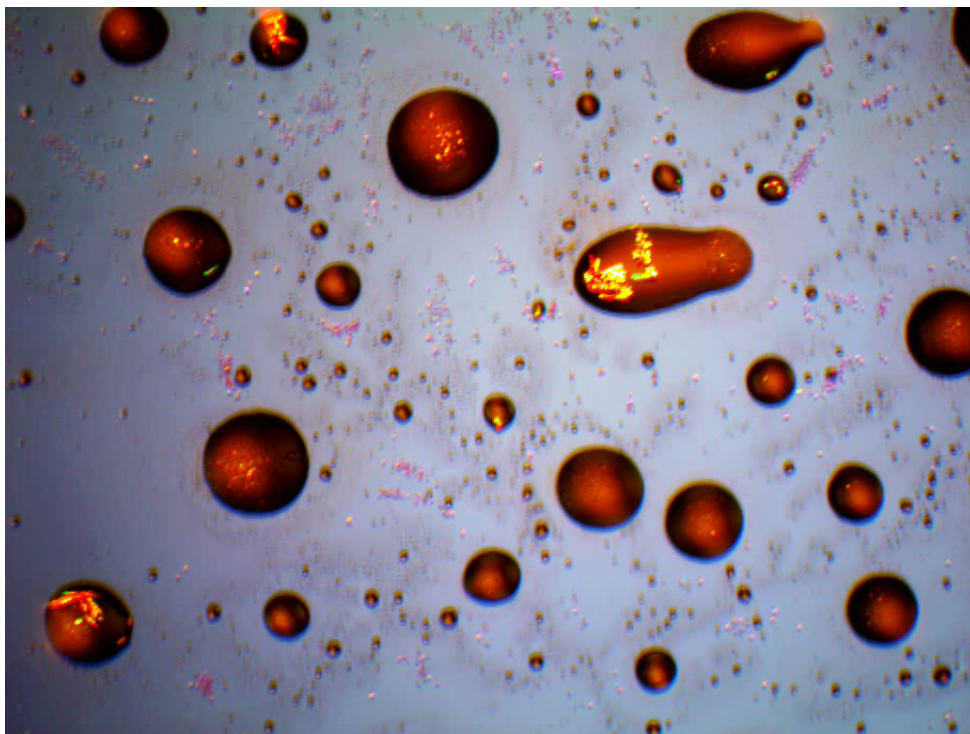
Figure 4.25: Birefringence appearing at 40 °C while a sample dries. Imaged under mixed cross-polarized and bright field conditions at 10x magnification.

As this was past the clearing point of 5CB, it could not have been the liquid crystal. Additionally, the sample had dried, which is why several of the vesicles in Figure 4.25 appear to have contact points with the glass slide. To further investigate what was causing birefringence at a temperature higher than the clearing point of the 5CB, a higher magnification phase contrast microscope was used. These images, as seen in Figure 4.26 show faceted structures that formed inside of the lipid vesicles.
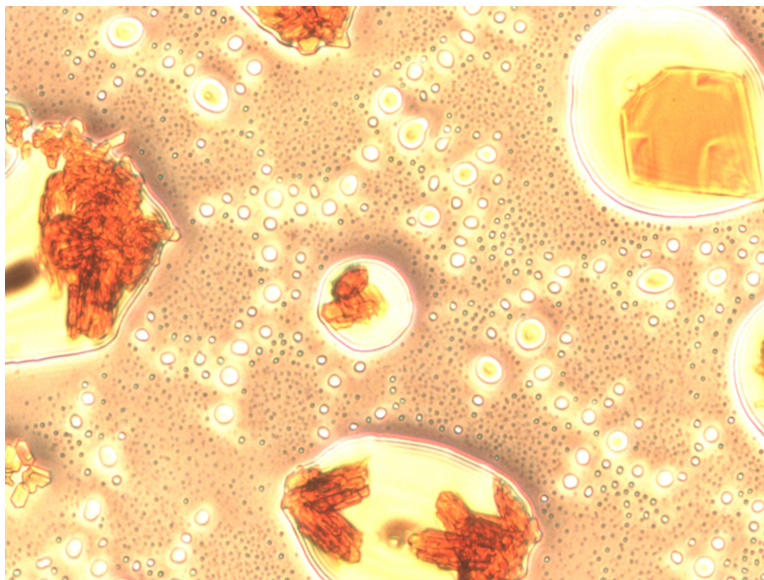
Figure 4.26: Faceted structures appearing in dried vesicle sample, imaged with phase contrast microscope at 20x magnification.

Although the structures had a clear geometric shape, it was not obvious what they were composed of. A fluorescent light source was used to get a better image of where the dye was located, as seen in Figure 4.27.
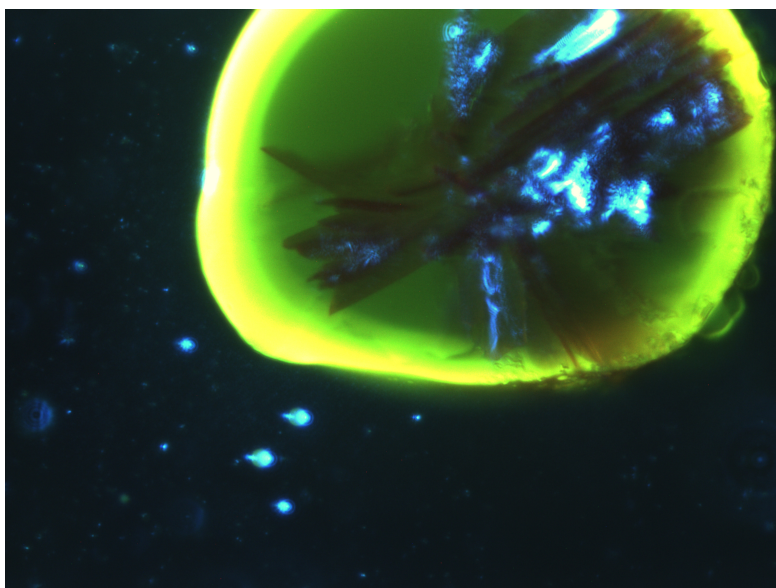
Figure 4.27: A fluorescent-phase contrast image of faceted structures at 40x magnification.

The green fluorescence is from the dye and the blue light is from the fluorescent light source,

however, the structure inside of the vesicle did not seem to fluoresce. At first, this seemed to indicate that the lipid forming in to crystal-like structures, as the dye in the vesicle wall was fluorescing. However, with little evidence to support this, images of the diI dye powder placed directly on a microscope slide were collected, as seen in Figure 4.28.
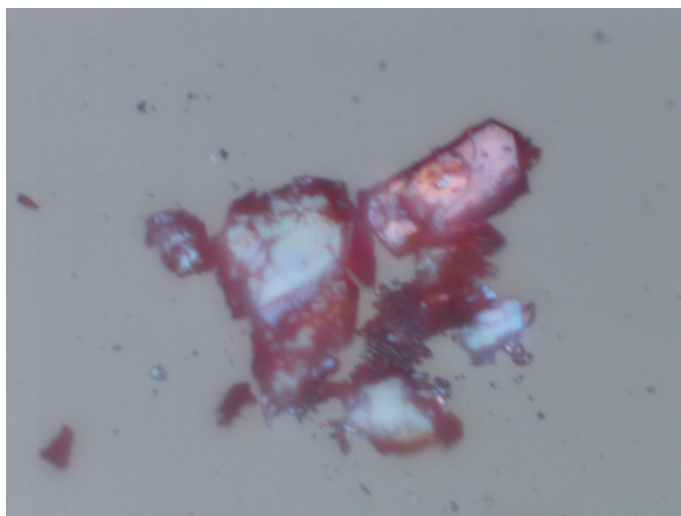
Figure 4.28: diI powder imaged directly on a microscope slide. Image taken with Nikon MM40 surface scan microscope at 20x magnification.

The dye seemed to have similar faceted structures, indicating that it was not the lipid crystallizing, but rather the dye. To confirm this, the same experiment was conducted with a solution containing a tenth of the amount of dye. There was still enough dye to stain the lipid, however, crystal-like structures were no longer present.

To further investigate the cause of this unique crystallization process, some parameters of the experiment were altered. Confirming what could be seen with many of the other samples, a sample dry was left to dry without heating. In these samples, faceted structures could not be seen, implying that the transition of the liquid crystal in to the isotropic phase has some effect. Additionally, sealed cells were used while heating samples and when maintained in an aqueous environment, the structures did not form. From this, it seems that rapid drying is required to form these crystal-like structures.

A paper written by Jeffrey Brake et. al. in 2003 refers to the possibility of a similar

phenomenon occurring [30]. In this paper, the authors were studying lipid bilayers that had been suspended on 5CB liquid crystal. The intention was to study biomolecular interactions at this interface. At the end of the paper, Brake states "This mechanism may offer new approaches for reporting the formation of organized protein and lipid domains, for rapid screening of solution conditions leading to crystallization of proteins at interfaces."

This procedure has potential for an exciting practical application. There is currently a large research interest in protein crystallography. Current methods to crystallize proteins often involve carefully balanced buffer solutions, precise temperature control, and can take weeks of work [31]. Some other techniques involve low temperatures facilitated by the use of liquid nitrogen. The crystals formed in the lipid-liquid crystal mixtures occurred formed in a matter of minutes and at high temperatures (40 °C). The chemical structure of the dye is similar to that of some proteins, so it is possible that the same procedure could be applied to proteins. Protein crystals are often used for x-ray crystallography experiments in drug development and also used in chemical purification processes.

4.6   Results with Proteins

To attempt to apply the heating and drying procedure discussed in the previous section to a protein, a Lipid-LC mixture was created with lysozyme as a replacement for the diI. As Figure 4.29 shows, vesicles still formed in the presence of the protein. Although the vesicles still appeared as spherical and similarly in size to previous samples, the liquid crystal structure appeared to be less ordered. Under cross-polarized conditions, there is no clearly identifiable cross pattern, indicating that although there is some nematic ordering, it is not as highly ordered as previous samples.
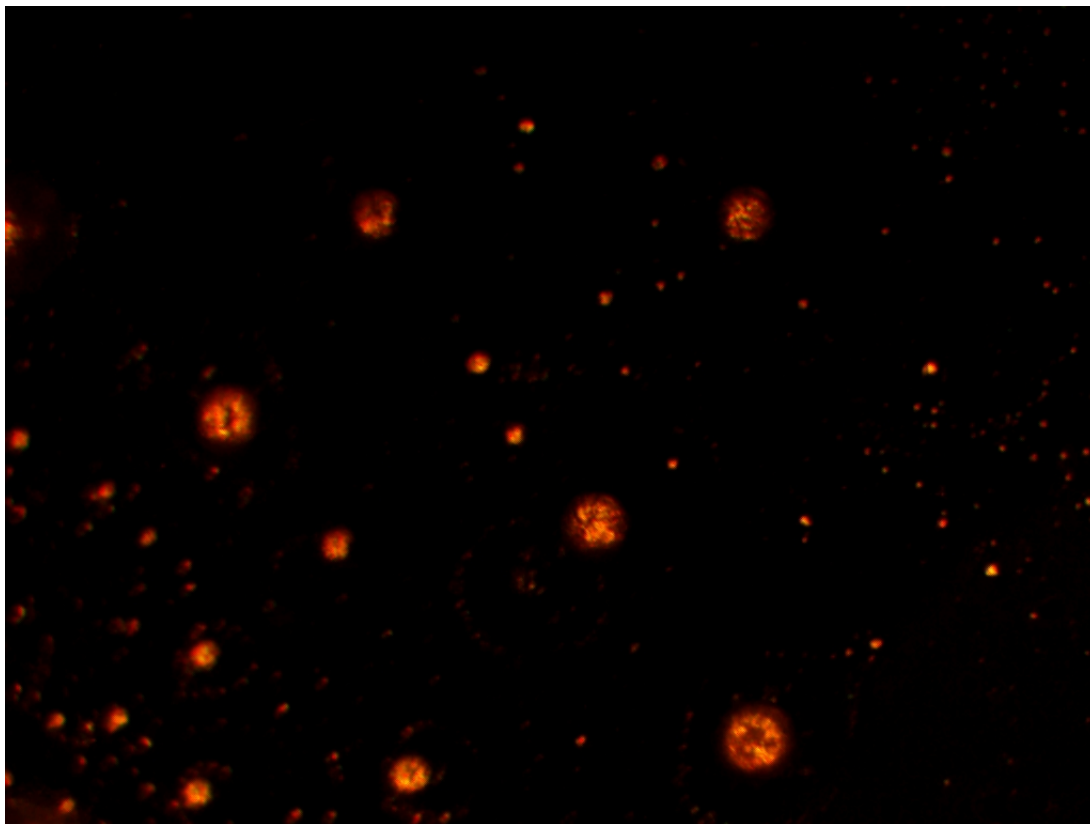
Figure 4.29: Vesicles formed in the presence of lysozyme at 24 °C. Imaged with cross-polarized microscope at 10x magnification.

As in previous experiments, the sample was dried on glass slide, rehydrated, heated to 40 °C and allowed to dry. Although crystal structures were not clearly visible, it appeared as if there were some aggregations within the vesicles. Additional experimentation and changes to sample concentrations would be needed to determine whether this procedure could be used to crystallize lysozyme. However, when looking at the sample on the cross-polarized microscope, something interesting began to occur. The outer ring of the collapsed vesicle occasionally became bright, indicating the formation of ordered structures. Eventually, it was discovered that breathing on the sample was causing the sudden birefringence. The likely cause is due to the moisture imparted to the sample while breathing. The hydrophobic ends of the 5CB were likely reacting to the presence of water and temporarily formed droplets. When the moisture evaporated, the liquid crystal relaxed and was no longer birefringent. Cross-polarized and bright field images of this process can be seen in Figure 4.30.

(a) Before Hydration, Cross Polarized

(b) Before Hydration, Bright Field

(c) After Hydration, Cross Polarized

(d) After Hydration, Bright Field
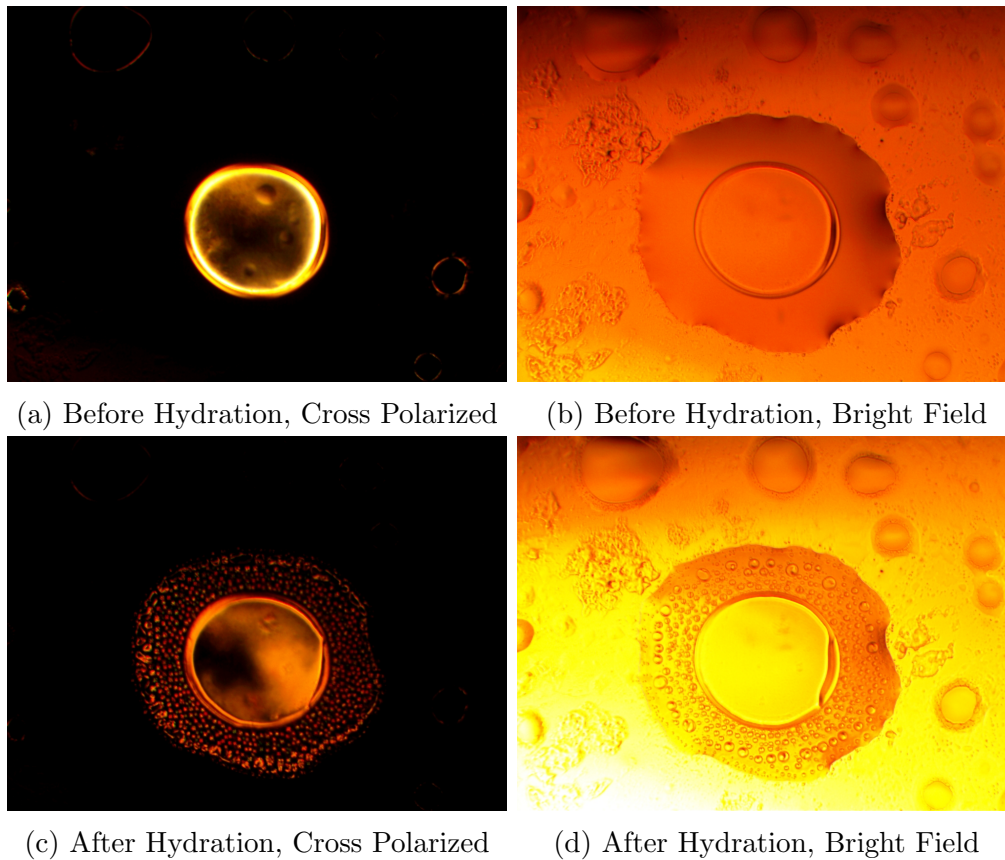
Figure 4.30: Lysozyme-liquid crytal mixture imaged after heating of the sample to 40 °C and allowing drying.

4.7 Turbidity with Fully Sealed Microscope Slide Cells

During the cross-polarized microscopy experiment, some samples never appeared to transition back to the nematic phase after being heated in to the isotropic phase and cooled. These samples had an unusual feature in that the sample sealed in the cell became a milky-white color. An example can be seen in Figure 4.31.
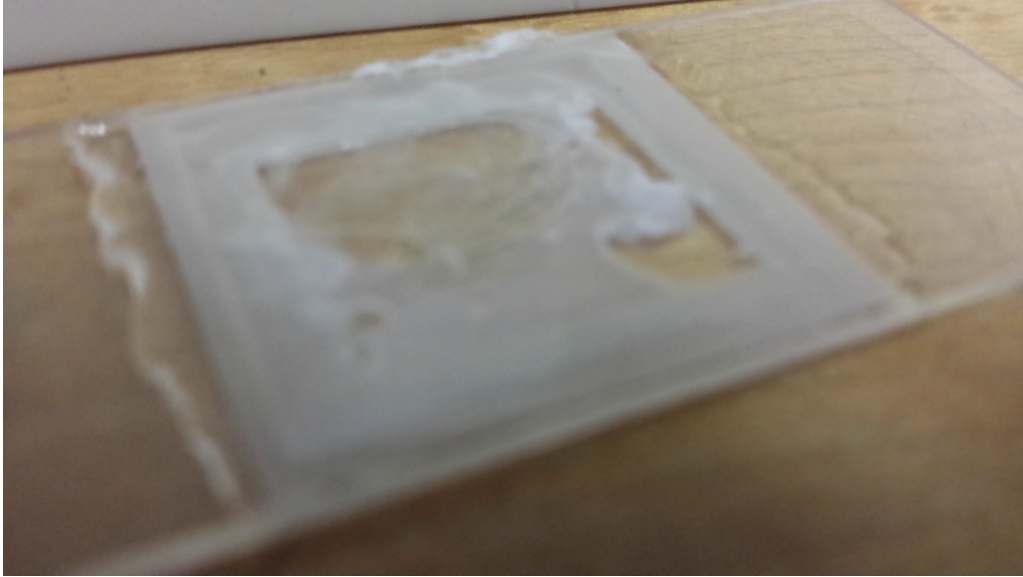
Figure 4.31: A turbid sample in a sealed microscope slide cell.

Most samples did not have this issue, indicating that the epoxy was not the cause. After occurring several times, it appeared as though the samples that became turbid were sealed best by the glass cover slip. Other samples would evaporate after several hours, however, some of the turbid samples retained the water for days or even weeks. Although unproven, it is possible that the nearly perfect seal on these samples created a near-vacuum inside the cell. Because the pressure was lowered so much, the water was able to boil at a low temperature, causing the turbid fluid in the cell.

5 Conclusions and Future Work

Lipid-liquid crystal mixtures show to have several possible applications in biotechnology research, and the behavior of the liquid crystal in lipid-liquid crystal mixtures as compared to its bulk properties proved to be complex. The most notable feature of these mixtures is the size of the vesicles formed using this procedure. The lipid seems to act as a surfactant to the oily liquid crystal droplets. Radially ordered nematic droplets of the 5CB liquid crystal allows for extremely large vesicles to form. To study the interesting behavior of this system, three main experiments were performed.

The first of these experiments was aimed at determining the size an distribution of the vesicles and was conducted using phase contrast microscopy. ImageJ was used to automate the analysis process. The mean diameter of the vesicles increased with increasing concentration of 5CB, however, the system proved to have bimodal structure. Collections of smaller vesicles ($\approx 80\mu$m) formed at all concentrations and this average did not vary much. Several larger vesicles formed at each concentration, and it was the size of the large vesicles that increased with increasing concentration of liquid crystal. This is likely due to the phase separation process of the liquid crystal from the solvents when the solvents evaporate.

The large vesicles could potentially be used as stand-ins for cell membranes in biological research. Model lipid vesicles are often used in this research, however, the standard vesicle creation procedures lead to much smaller vesicles. Other techniques to create large vesicles use oily droplets, which the lipid coats. However, most oils do not have properties similar to water. When 5CB is heated into the isotropic phase, it has a similar density and behavior to water. To determine the feasibility of using lipid-liquid crystal mixtures for bioresearch, studies would have to be conducted to determine how similar vesicles containing 5CB behave to those containing pure water.

The second experiment was aimed at studying the phase-transition of the 5CB liquid crystal by using cross-polarized microscopy. By analyzing the mean intensity of images that correspond with a certain temperature, the phase transition temperature of the liquid crystal

could be determined. Using image analysis techniques, this experiment had the benefit of not only being able to determine the transition temperature of the entire system, but also that of individual vesicles. By analyzing different size vesicles, a trend was identified. Size effects began to dominate smaller vesicles, and thus the liquid crystal would transition at a lower temperature. However, between samples at different concentrations, this trend did not directly correlate. This suggests that the size of the vesicle did not purely determine the phase transition temperature. There was likely some materials dissolved in the liquid crystal, altering the transition temperature differently for each sample. Additionally, there was possibly some diffusion occurring, also having an effect on the transition temperature.

A third experiment was aimed at probing the the phase transitions of lipid-liquid crystal mixtures using modulated differential scanning calorimetry. In addition, this technique allowed for study of the energetics of the entire system. Because of the system's complexity, the data collected was not systematic and therefore difficult to interpret. Several trials contained large spikes correlating to the phase transition of the liquid crystal, however, additional heat signatures were detected throughout the temperature scans. This behavior could be attributed to the lipid, dye, water, or any interactions or rearrangement of these components.

The largest source of error in the calorimetry experiments was introduced by the sample preparation procedure. Vesicles did not form directly in the calorimetry pans, so they had to be synthesized on a glass slide and then scraped in to the pan. The scraping distributed the sizes of the vesicles unpredictably and may have destroyed some of the vesicles. This might be one of the reasons, the phase transition temperatures found using calorimetry did not correlate well with the cross-polarized microscopy experiment. To gather more accurate results, a new procedure would have to be devised. Either the scraping procedure would have to be changed or improved such that all of the sample could be harvested without any damage to the vesicles.

In addition to these experiments, several previously unseen phenomena were observed.

Most notably, in samples containing an excess of dye, the dye crystallized in the droplets of liquid crystal when the sample was heated and allowed to dry. This may occur as a large concentration gradient is introduced when the water evaporates. It was also discovered that the liquid crystal had to be in the isotropic phase for the dye to crystallize. If this crystallization procedure can be adapted to other substances, it may have some exciting practical implications. Protein crystallography is a large field of research, and current methods to produce protein crystals are slow and require very precise chemical processes and low temperatures. The crystallization that occurred in the lipid-liquid crystal mixtures happened on a very short time scale and at high temperature.

The work done so far with lipid-liquid crystal mixtures has introduced many new phenomena. This leaves room for a lot of further work on the subject. The dye crystallization phenomenon could have important practical applications, and further study is required to understand the mechanism at work and to try crystallizing other substances. More information could also be gathered from calorimetry, however, a better vesicle harvesting procedure would need to be implemented. Another interesting feature that could possibly be studied with calorimetry would be the gel-liquid phase transition that the lipid undergoes at approximately -3 °C [32]. A lower temperature scan would be required to study this behavior. Finally, this thesis shows that by using liquid crystal droplets,extremely large lipid vesicles can be easily created which could have practical biophysical research applications.

References

[1] Chiranjeevi Peetla, Andrew Stine, and Vinod Labhasetwar. Biophysical interactions with model lipid membranes: Applications in drug discovery and drug delivery. *Molecular Pharmeceutics*, 6(5):1264–1276, 2009.

[2] Donald Voet, Judith Voet, and Charlotte Pratt. *Fundamentals of Biochemistry*. Wiley & Sons, 3 edition, 2008.

[3] Yukihisa Okumura, Hao Zhang, Takuya Sugiyama, and Yuuichi Iwata. Electroformation of giant vesicles on a non-electroconductive substrate. *Journal of the American Chemical Society*, 129(6):1490–1491, 2007.

[4] S. Chandrasekhar. *Liquid Crystals*. Cambridge University Press, New York, NY, 1992.

[5] Birendra Bahadur. *Liquid Crystals Applications and Uses*, volume 1. World Scientific Publishing, River Edge, NJ, 1990.

[6] Parvathalu Kalakonda. *Thermal Physical Properties of Nanocomposites of Complex Fluids*. Dissertation, 2013.

[7] Alberta Ferrarini, Silvia Pieraccini, Stefano Masiero, and Gian Piero Spada. Chiral amplification in a cyanobiphenyl nematic liquid crystal doped with helicene-like derivatives. *Beilstein Journal of Organic Chemistry*, 5(50), 2009.

[8] T. Bezrodna, V. Melnyk, V. Vorobjev, and G. Puchkovska. Low-temperature photoluminescence of 5cb liquid crystal. *Journal of Luminescence*, 130:1134–1141, 2010.

[9] Samaneh Mashaghi, Tayebeh Jadidi, Gijsje Koenderink, and Alireza Mashaghi. Lipid nanotechnology. *International Journal of Molecular Sciences*, 14:4242–4282, 2013.

[10] David Fankhauser, 2013.

[11] http://www.supplementclinic.com/.

[12] http://antranik.org/.

[13] Nam-Joon Cho, Lisa Hwang, Johan Solandt, and Curtis Frank. Comparison of extruded and sonicated vesicles for planar bilayer self-assembly. *Materials*, 6:3294–3308, 2013.

[14] B. J. Frisken, C. Asman, and P.J. Patty. Studies of vesicle extrusion. *Langmuir*, 16(3):928–933, 1999.

[15] Wojciech Zielenkiewicz and Eugeniusz Margas. *Theory of Calorimetry.* Kluwer Academic Publishers, New York, NY, 2004.

[16] Nihar Pradhan. *Thermal Conductivity of Nanowires, Nanotubes And Polymer-Nanotube Composites.* Thesis, 2010.

[17] TA Instruments. Modulated differential scanning calorimetry, 2014.

[18] Sindee Simon. Temperature-modulated differential scanning calorimetry: theory and application. *Thermochimica Acta*, 374(1):55–71, 2001.

[19] Leonard Thomas. Modulated dsc paper #2 modulated dsc basics; calculation and calibration of mdsc signals, 2005.

[20] Douglas Murphy, Kenneth Spring, and Michael Davidson. Introduction to polarized light, 2013.

[21] Philip Robinson and Michael Davidson. Introduction to polarized light microscopy, 2013.

[22] Kenneth Spring and Michael Davidson. Introduction to fluorescence microscopy, 2013.

[23] Douglas Murphy, Ron Oldfield, Stanley Schwartz, and Michael Davidson. Introduction to phase contrast microscopy, 2013.

[24] Eclipse te 300, 1998.

[25] 10mp microscope digital camera compatible w/ windows & mac os, 2013.

[26] Caroline Schneider, Wayne Rasband, and Kevin Eliceire. Nih image to imagej: 25 years of image analysis. *Nature Methods*, 9:671–675, 2012.

[27] Greg McHone. Ernst leitz wetzlar microscopes, 2011.

[28] 3mp usb2.0 microscope digital camera + software, 2013.

[29] Inc. Lake Shore Cryotronics. User's manual model 340 temperature controller, 2004.

[30] Jeffrey Brake, Maren Daschner, Yan-Yeung Luk, and Nicholas Abbott. Biomolecular interactions at phospholipid-decorated surfaces of liquid crystals. *Science*, 302:2094–2097, 2003.

[31] Dave Lawson. A brief introduction to protein crystallography, 2012.

[32] Sukit Leekumjorn and Amadeu Sum. Molecular characterization of gel and liquid-crystalline structures of fully hydrated popc and pope bilayers. *The Journal of Physical Chemistry*, 111(21):6026–6033, 2007.

Appendices

A   Materials

- 2-Oleoyl-1-palmitoyl-sn-glycero-3-phosphocholine (POPC): Obtained from Sigma-Aldrich. A self-assembling lipid found in eukaryotic cell membranes. Molecular Weight 760.08.

- 3,3'-Dihexyloxacarbocyanine iodide (diI): Obtained from Sigma-Aldrich. A fluorescent protein labeling dye. Has an excitation wavelength of 485 nm and emission wavelength of 501 nm. Molecular Weight 572.52 .

- Methanol: Obtained from Sigma-Aldrich. Anhydrous grade solvent. 99.8% assay.

- Chloroform: Obtained from Sigma-Aldrich. Anhydrous grade solvent. $\geq$ 99% assay.

- 4-Cyano-4'-pentylbiphenyl (5CB): Obtained from Frinton Laboratories Inc., Vineland, NJ. Molecular weight 249.36. Aspect ratio 2 nm: 0.5 nm.

B   ImageJ Macro

```
inputFolder = getDirectory("C:\\Users\\petersj\\Documents\\Thesis\\5CB\\1%5CB_4x");

outputFolder = getDirectory("C:\\Users\\petersj\\Documents\\Thesis\\5CB\\1%5CB_Results")

images = getFileList(inputFolder);

for (i=0; i<images.length; i++) {

 inputPath = inputFolder + images[i];

 open(inputPath);

//run("Threshold...");


setOption("BlackBackground", false);

run("Make Binary");

run("Analyze Particles...", "size=6000-Infinity circularity=0.2-1.00 show=Ellipses

    exclude clear include");

setAutoThreshold("Default");

//run("Threshold...");

run("Close");

run("Analyze Particles...", "size=6000-Infinity circularity=0.20-1.00 show=Masks

    display exclude clear include");

selectWindow("Results");

saveAs(".txt",inputPath);

close();

close();

if (isOpen("Results")) {

      selectWindow("Results");

      run("Close");

   }

}
```

C   Calorimetry Data Overlays
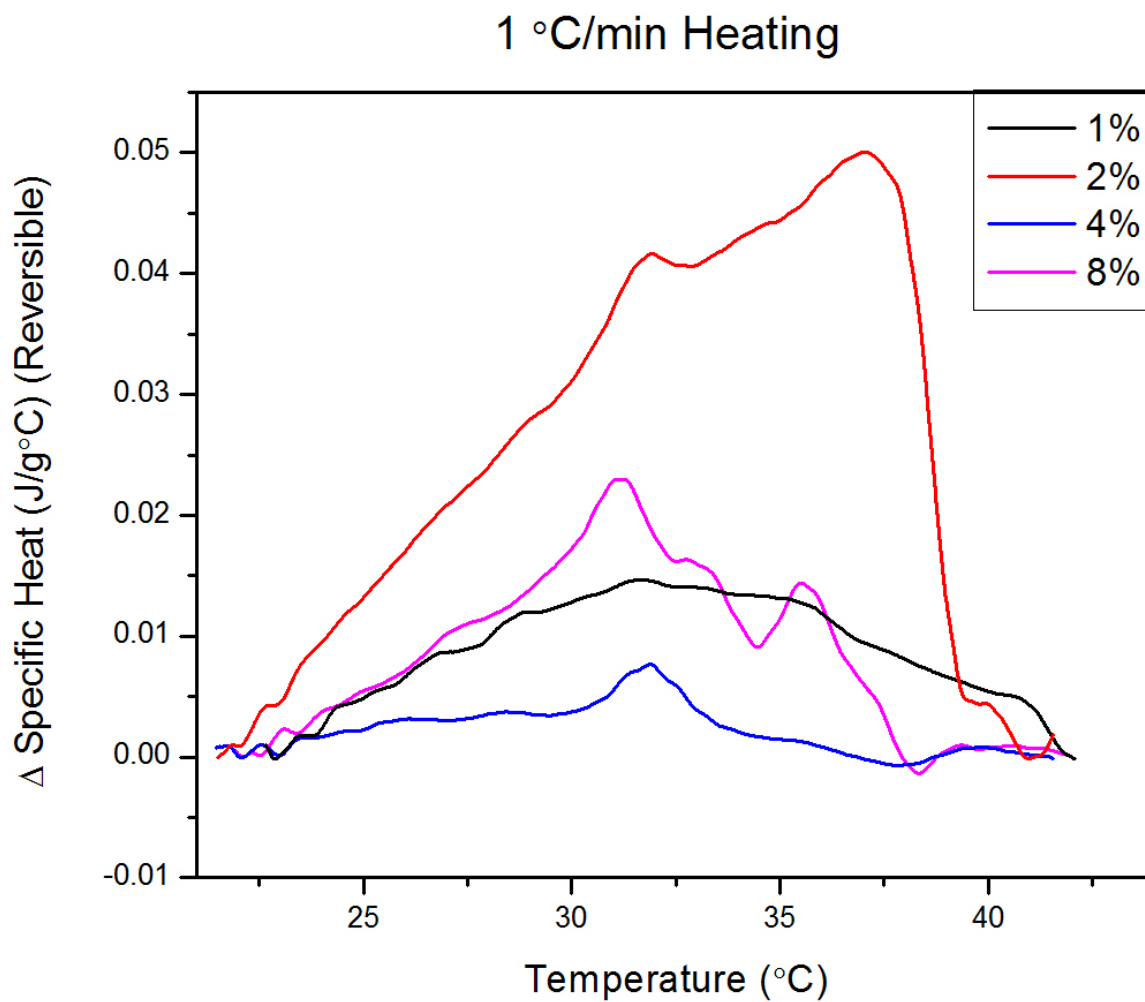
Figure C.1: An overlay of reversible specific heat data for different concentrations of 5CB, with a 1 °C/min scan rate.
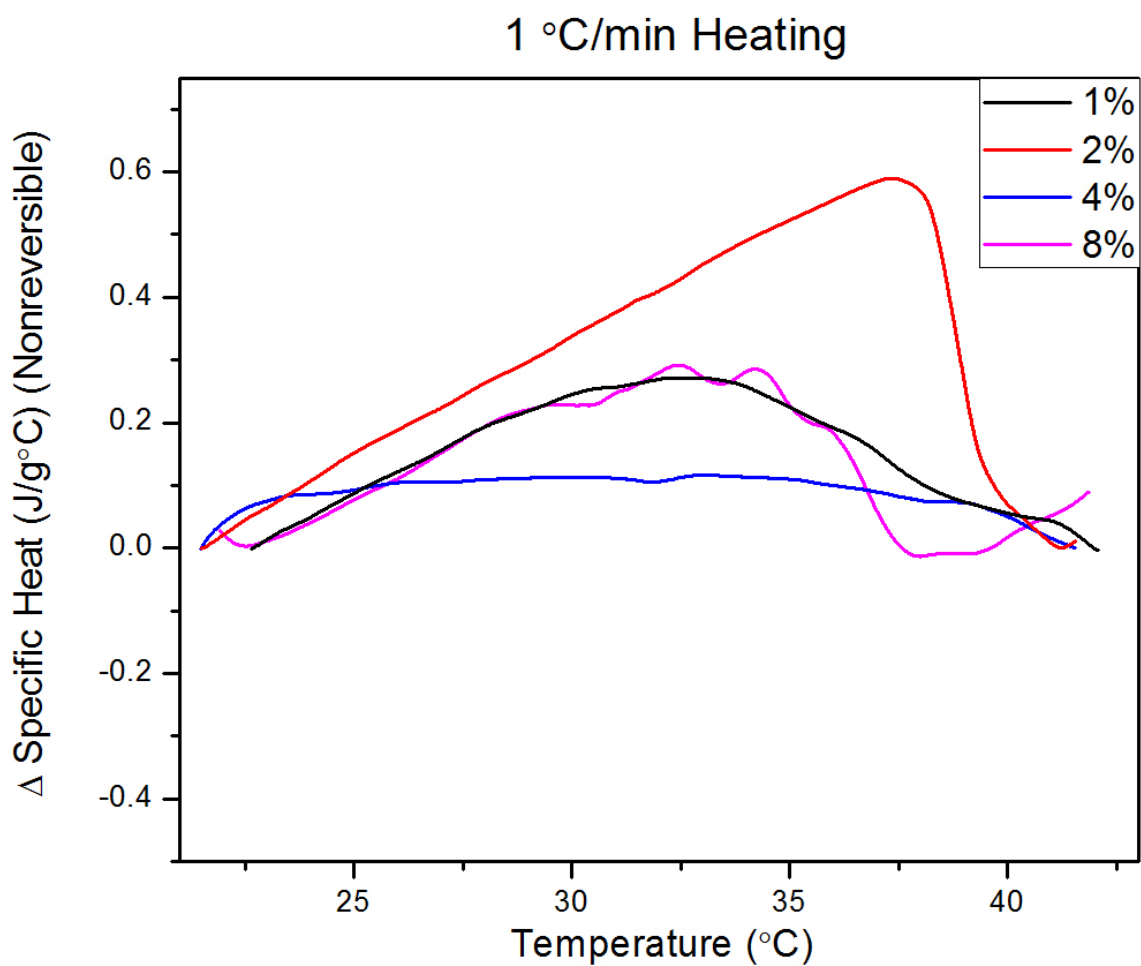
Figure C.2: An overlay of nonreversible specific heat data for different concentrations of 5CB, with a 1 °C/min scan rate.
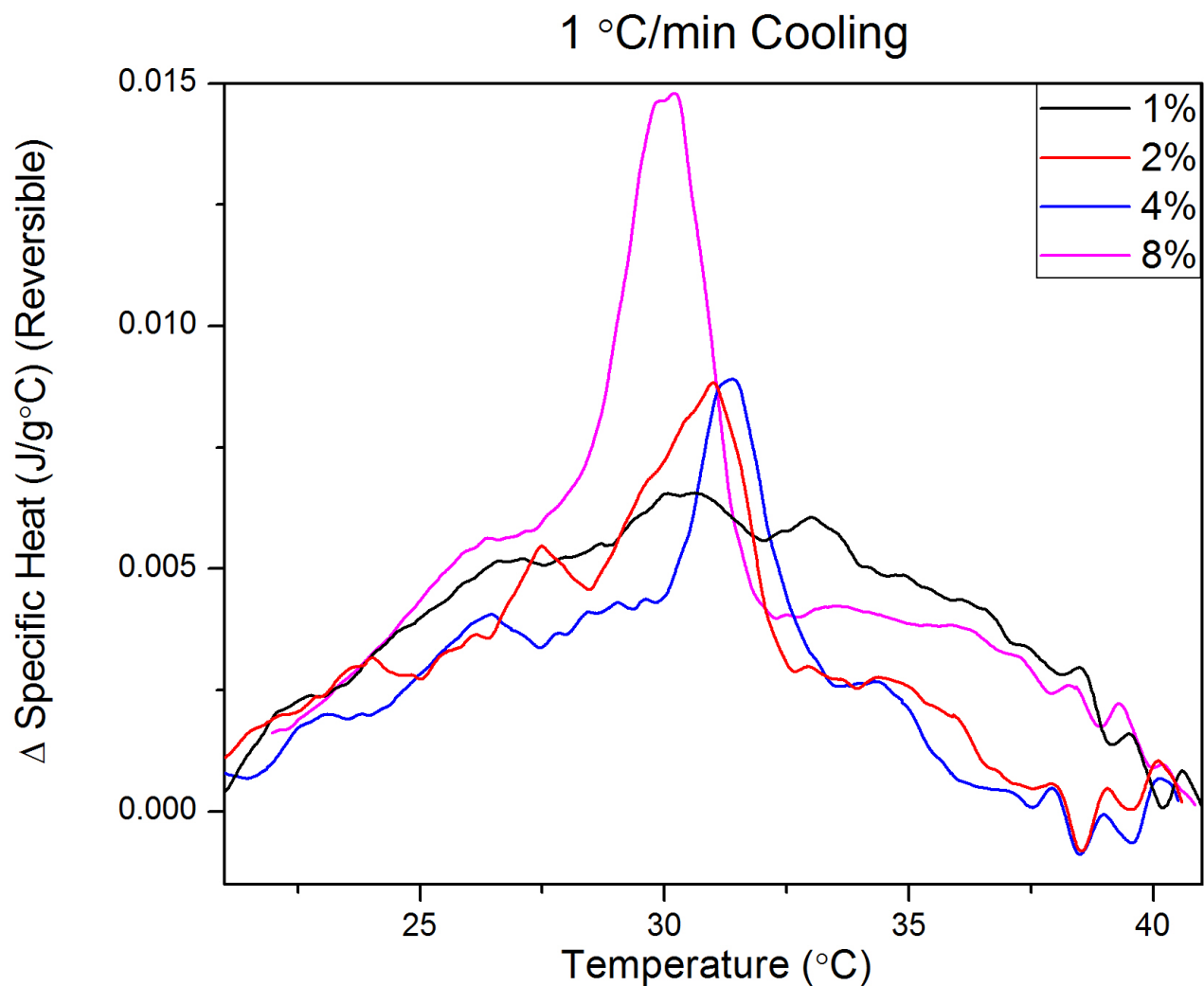
Figure C.3: An overlay of reversible specific heat data for different concentrations of 5CB, with a 1 °C/min scan rate.
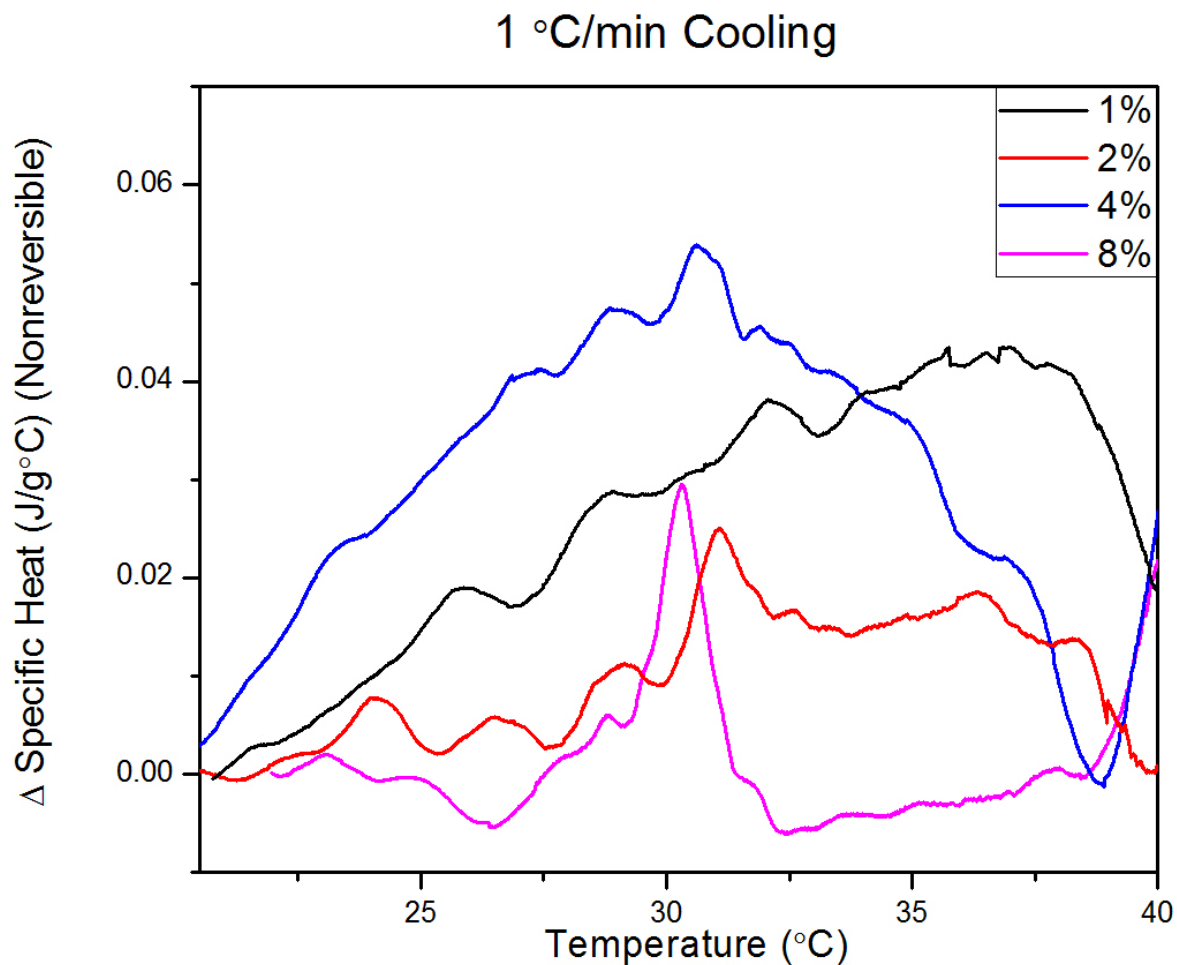
Figure C.4: An overlay of nonreversible specific heat data for different concentrations of 5CB, with a 1 °C/min scan rate.
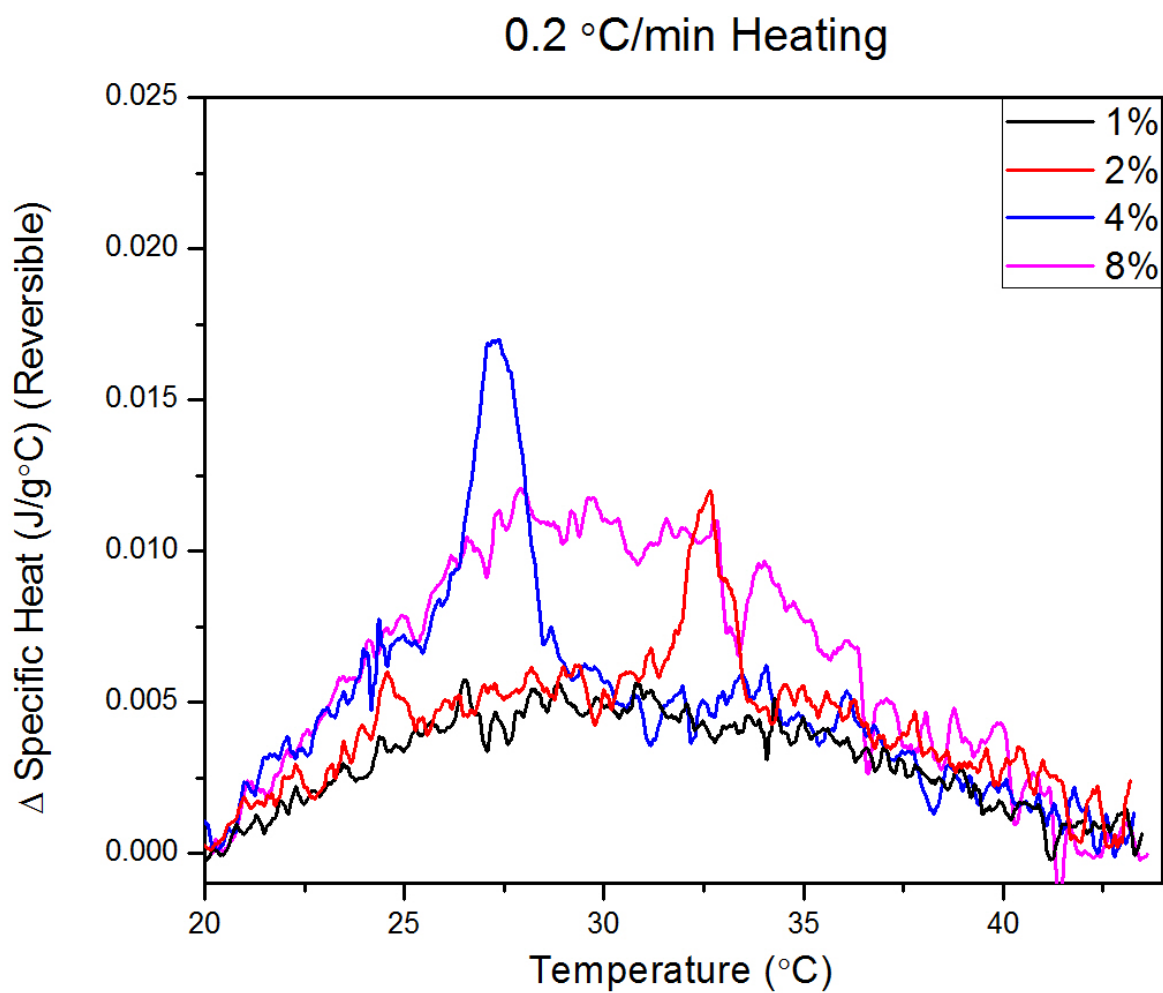
Figure C.5: An overlay of reversible specific heat data for different concentrations of 5CB, with a 0.2 °C/min scan rate.
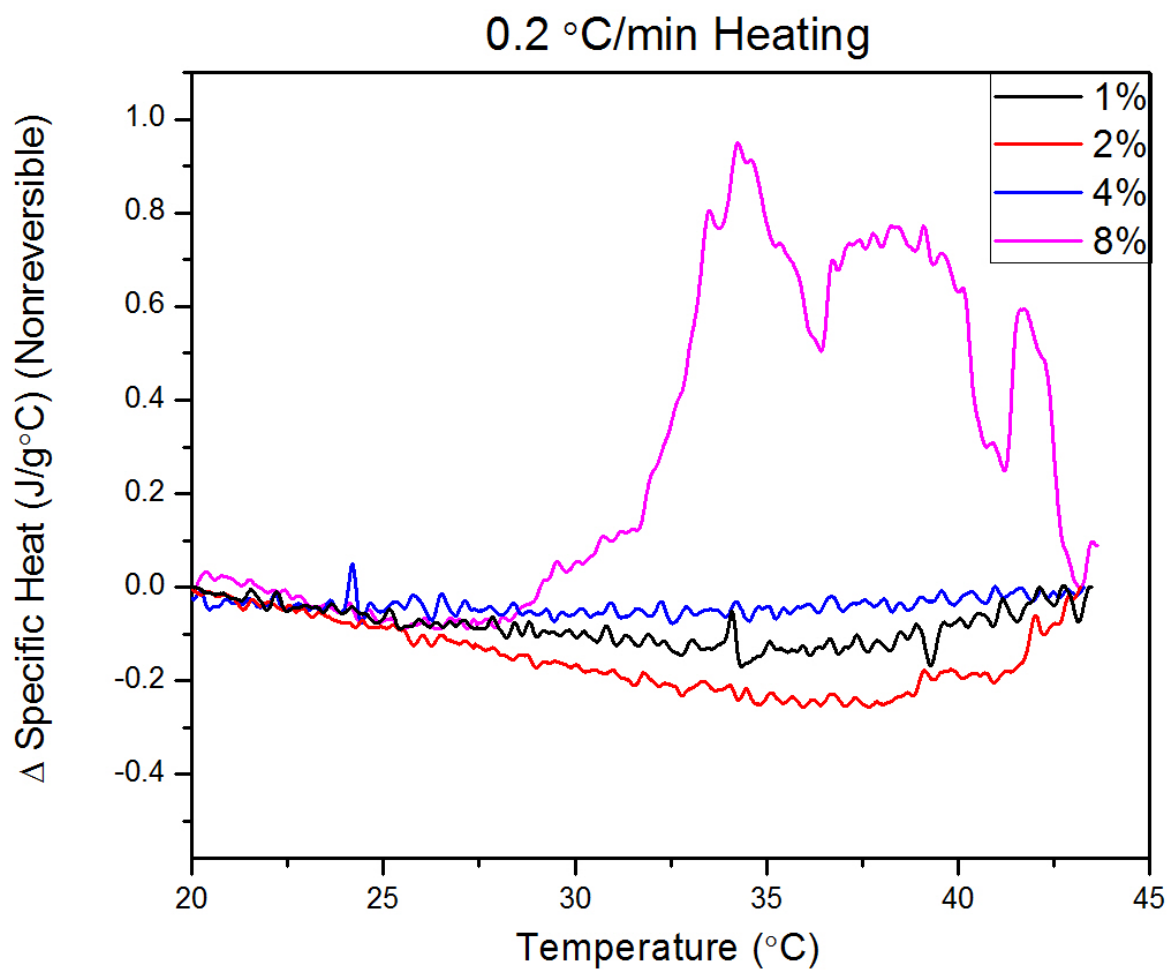
Figure C.6: An overlay of nonreversible specific heat data for different concentrations of 5CB, with a 0.2 °C/min scan rate.
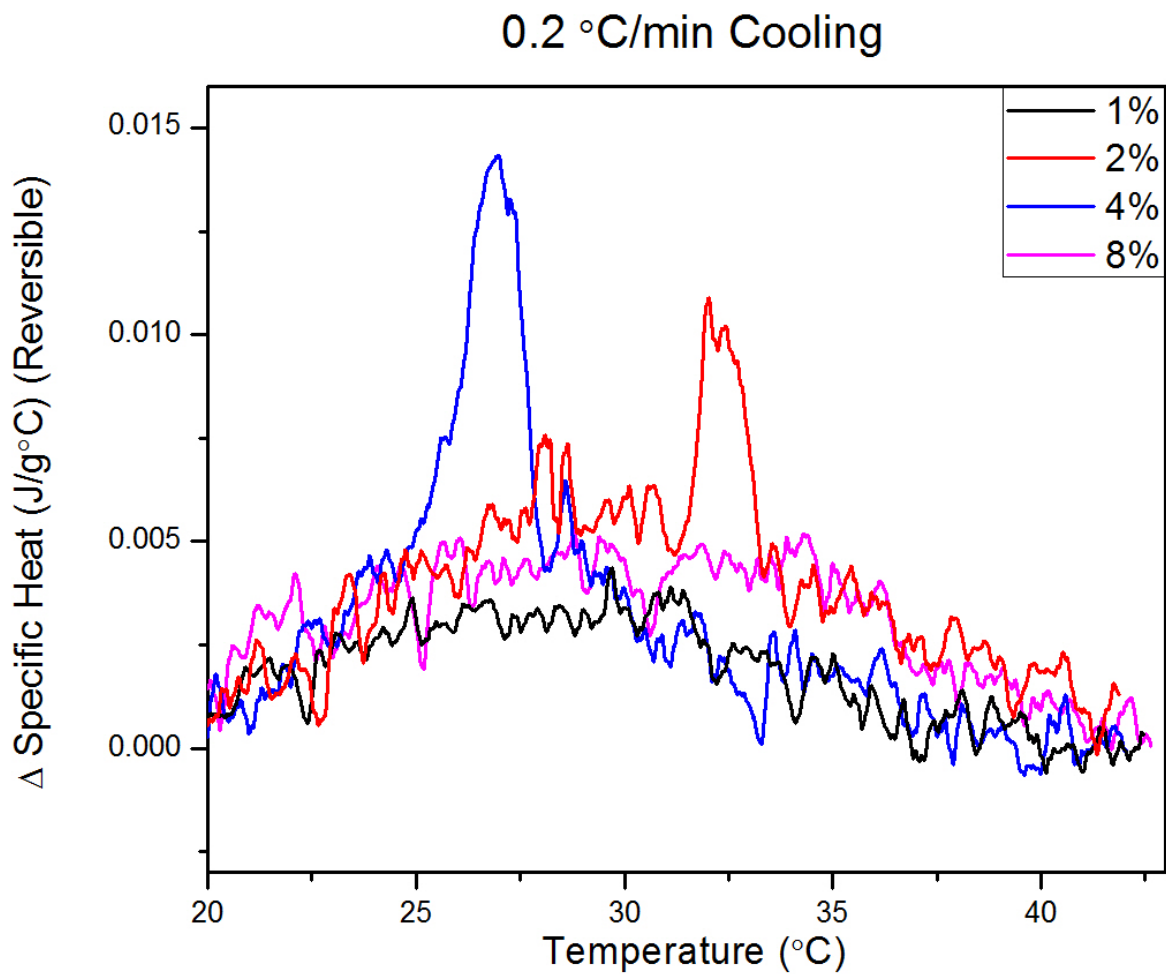
Figure C.7: An overlay of reversible specific heat data for different concentrations of 5CB, with a 0.2 °C/min scan rate.
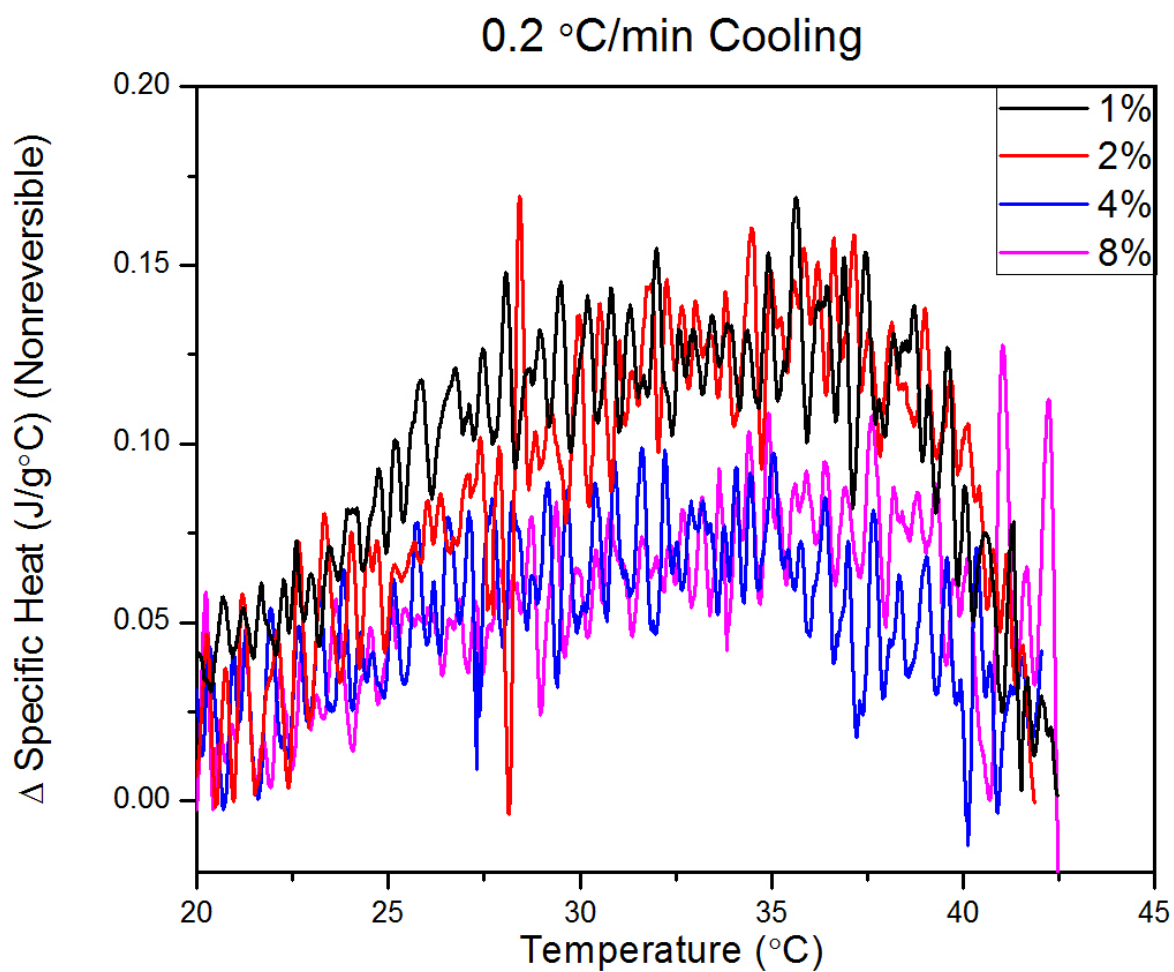
Figure C.8: An overlay of nonreversible specific heat data for different concentrations of 5CB, with a 0.2 °C/min scan rate.

D Calorimetry Data Hysteresis
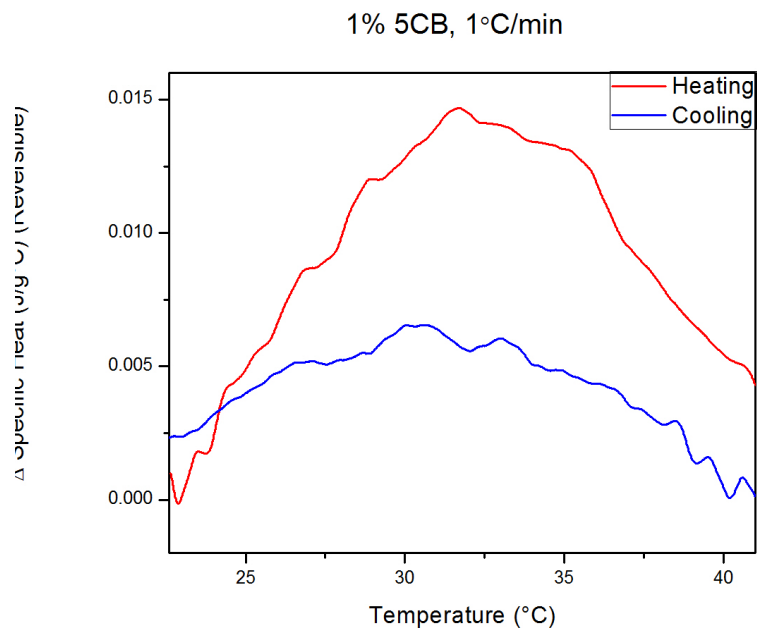
Figure D.1: A hysteresis plot of reversible specific heat data for 1% 5CB with a 1 °C/min scan rate.
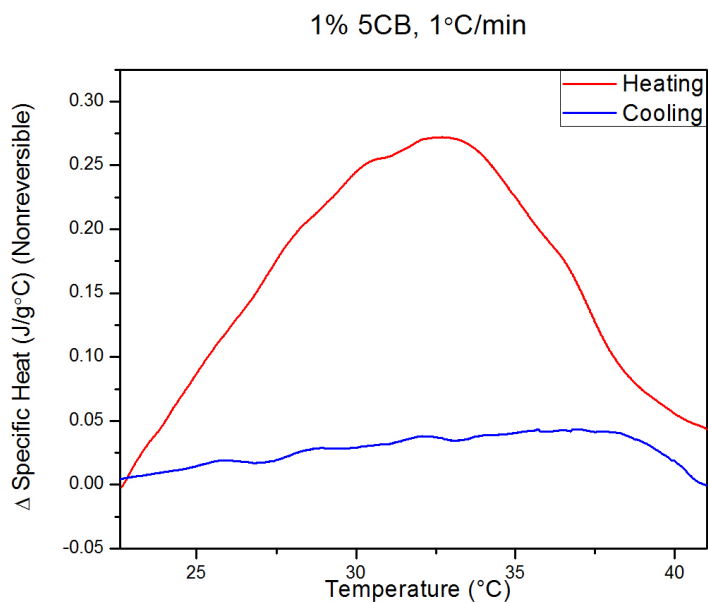
Figure D.2: A hysteresis plot of nonreversible specific heat data for 1% 5CB with a 1 °C/min scan rate.
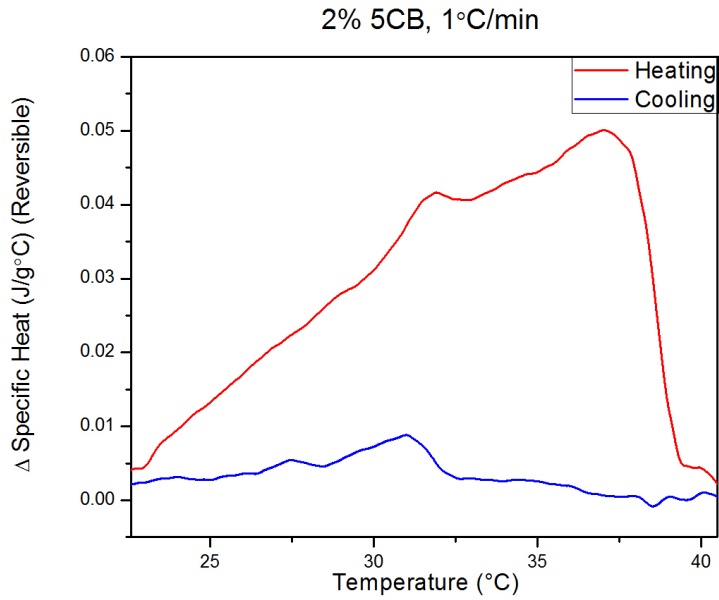
Figure D.3: A hysteresis plot of reversible specific heat data for 2% 5CB with a 1 °C/min scan rate.
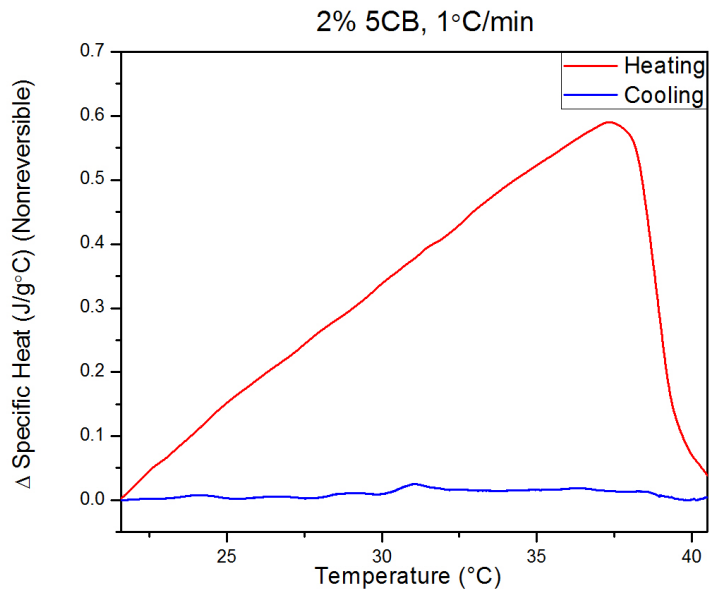
Figure D.4: A hysteresis plot of nonreversible specific heat data for 2% 5CB with a 1 °C/min scan rate.
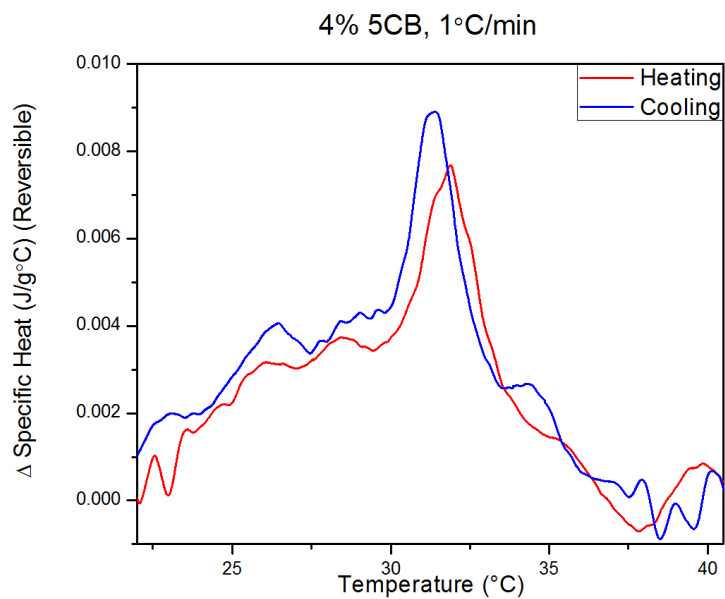
Figure D.5: A hysteresis plot of reversible specific heat data for 4% 5CB with a 1 °C/min scan rate.
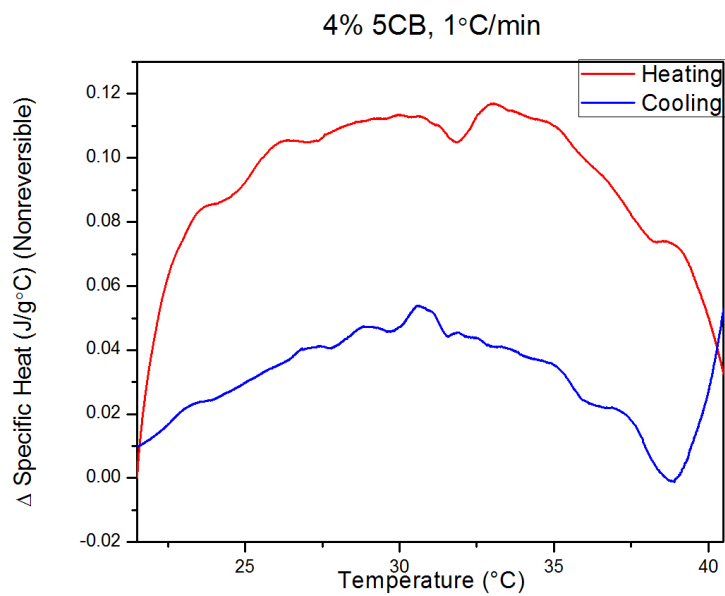
Figure D.6: A hysteresis plot of nonreversible specific heat data for 4% 5CB with a 1 °C/min scan rate.
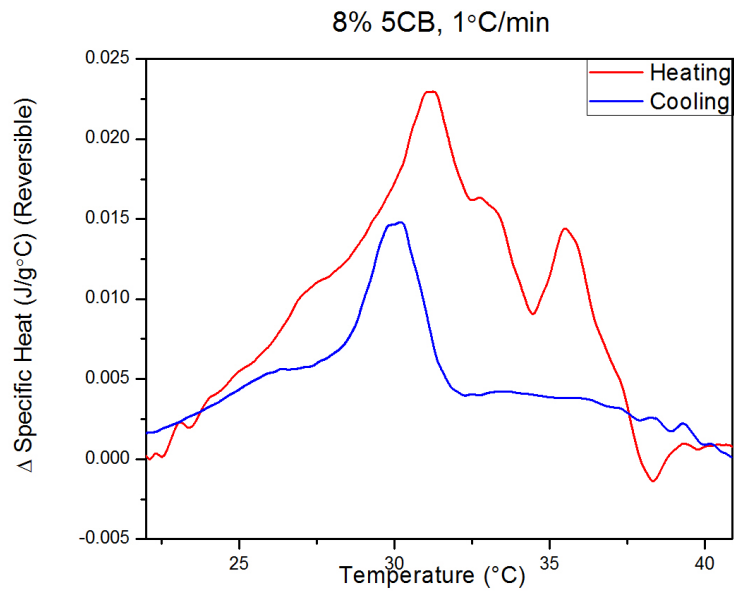
Figure D.7: A hysteresis plot of reversible specific heat data for 8% 5CB with a 1 °C/min scan rate.
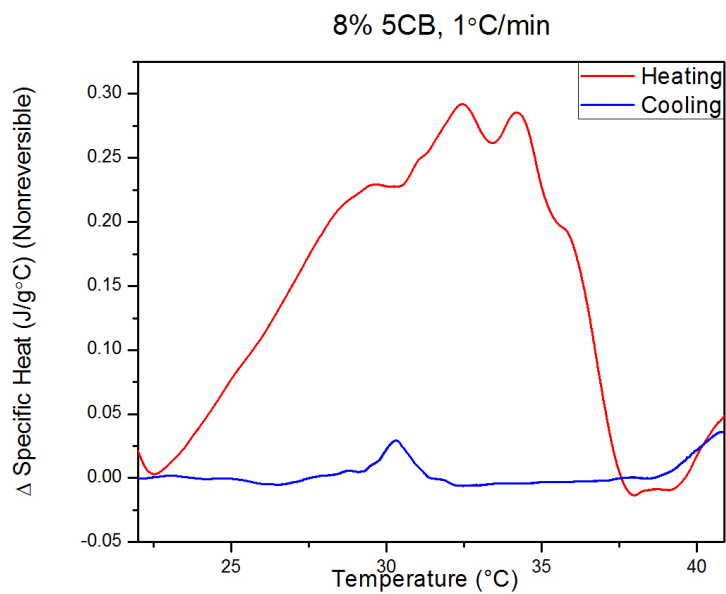
Figure D.8: A hysteresis plot of nonreversible specific heat data for 8% 5CB with a 1 °C/min scan rate.
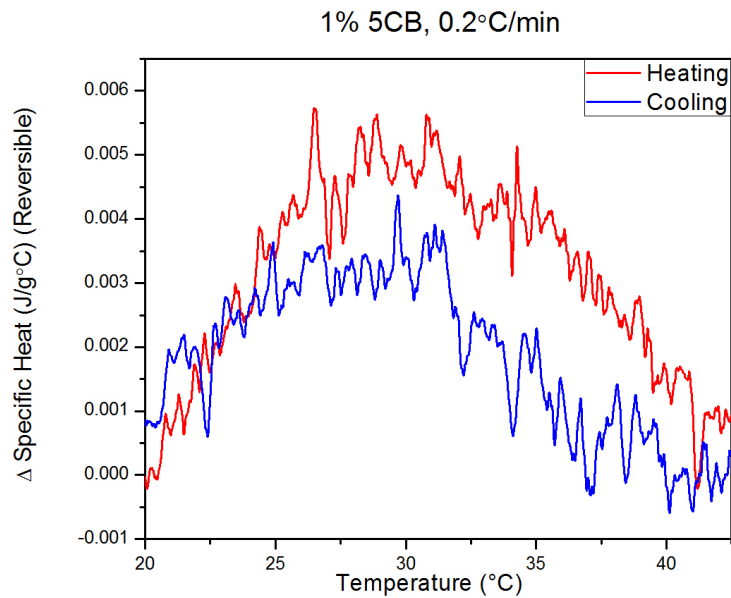
Figure D.9: A hysteresis plot of reversible specific heat data for 1% 5CB with a 0.2 °C/min scan rate.
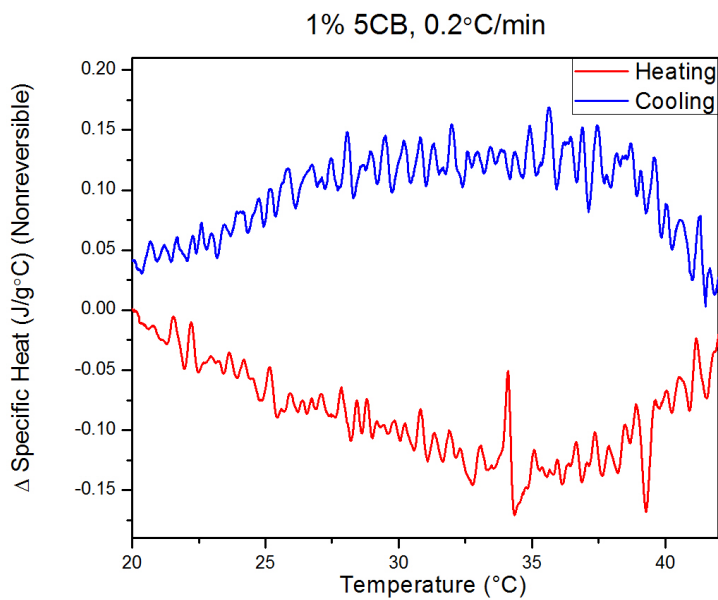
Figure D.10: A hysteresis plot of nonreversible specific heat data for 1% 5CB with a 0.2 °C/min scan rate.
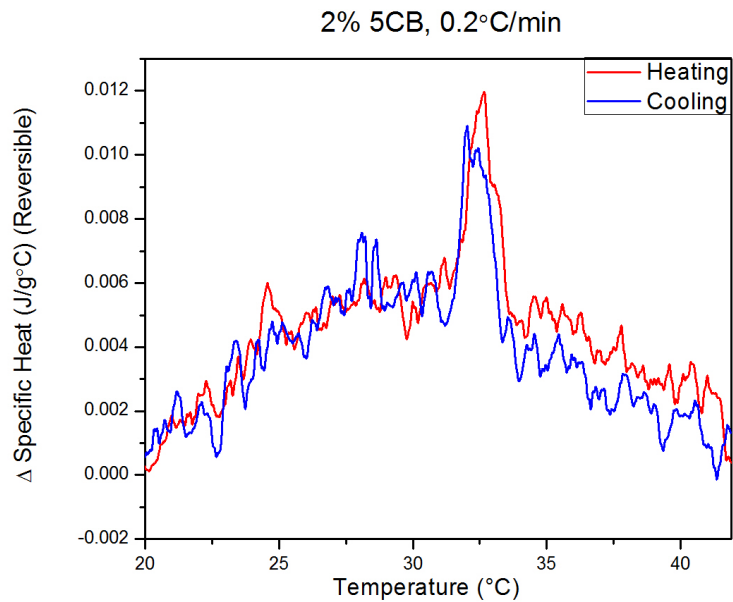
Figure D.11: A hysteresis plot of reversible specific heat data for 2% 5CB with a 0.2 °C/min scan rate.
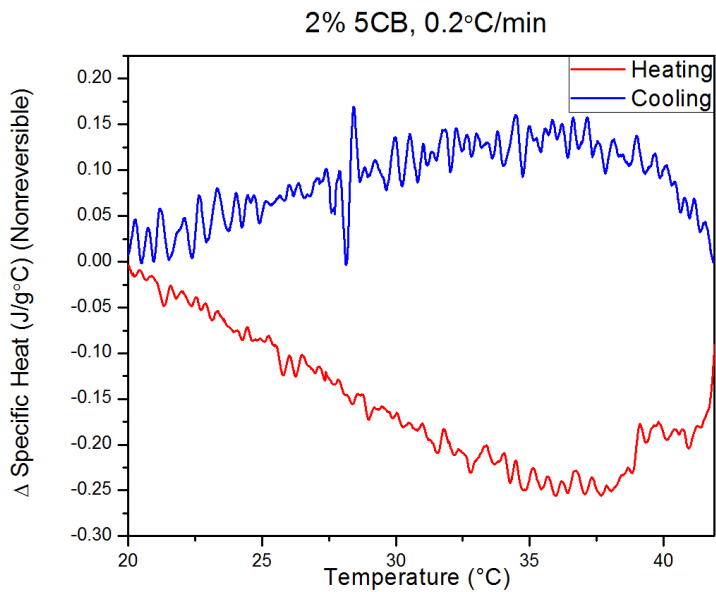
Figure D.12: A hysteresis plot of nonreversible specific heat data for 2% 5CB with a 0.2 °C/min scan rate.
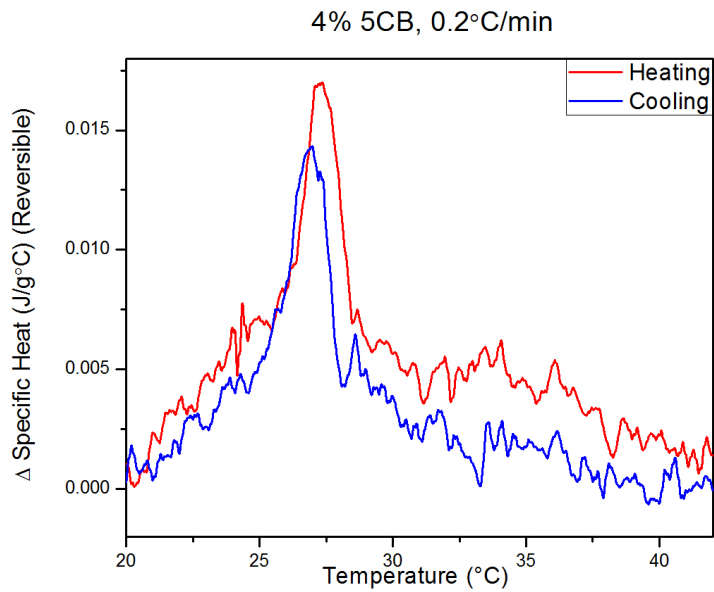
Figure D.13: A hysteresis plot of reversible specific heat data for 4% 5CB with a 0.2 °C/min scan rate.
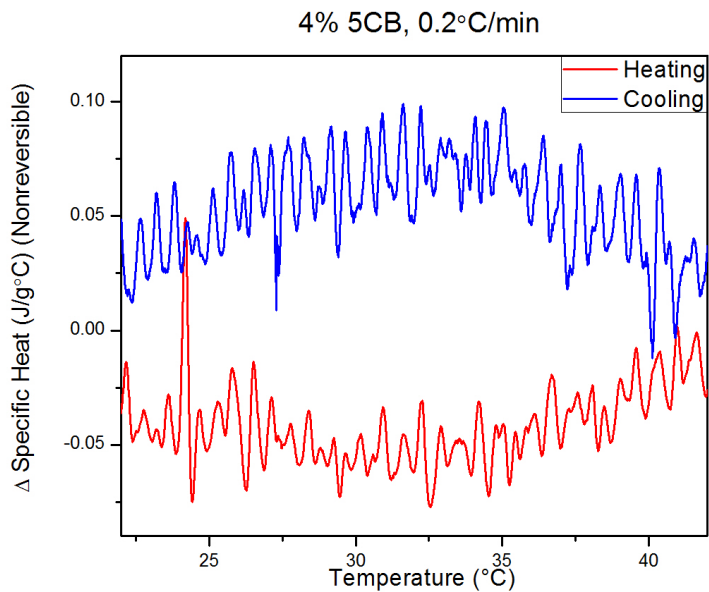
Figure D.14: A hysteresis plot of nonreversible specific heat data for 4% 5CB with a 0.2 °C/min scan rate.
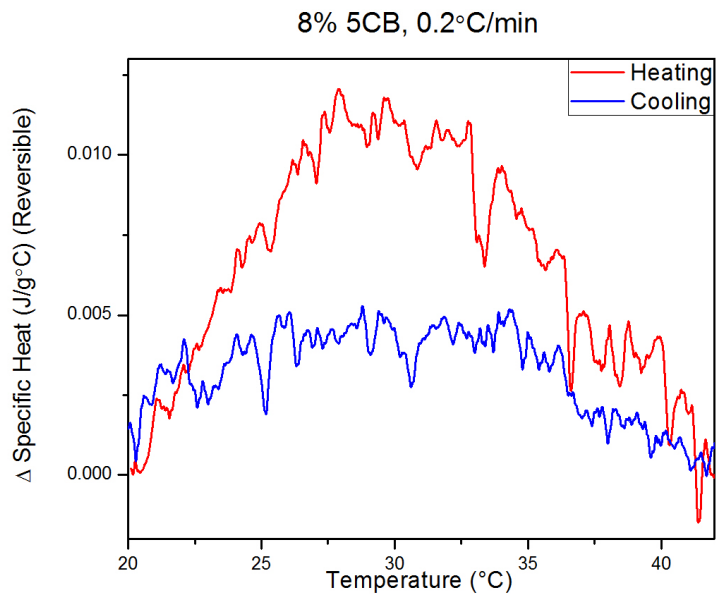
Figure D.15: A hysteresis plot of reversible specific heat data for 8% 5CB with a 0.2 °C/min scan rate.
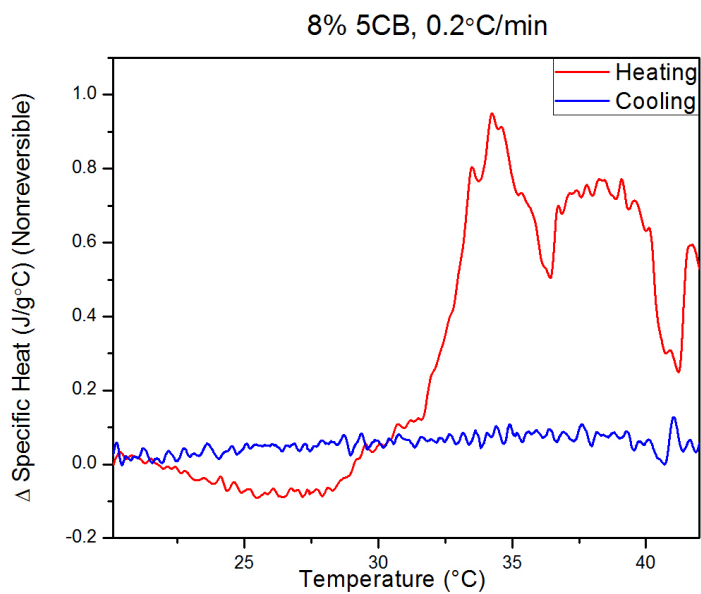
Figure D.16: A hysteresis plot of nonreversible specific heat data for 8% 5CB with a 0.2 °C/min scan rate.